Direct Nuclear Reactions

Carlos A. Bertulani and Angela Bonaccorso

Contents

Abstract

In this brief review, we discuss the basic theoretical concepts used in the experimental studies of the most common cases of direct reactions such as (a) elastic scattering, (b) inelastic scattering, (c) Coulomb excitation, (d) transfer reactions, and (e) breakup reactions.

C. A. Bertulani (✉)
Department of Physics and Astronomy, Texas A&M University-Commerce, Commerce, TX, USA
e-mail: carlos.bertulani@tamuc.edu

A. Bonaccorso
Istituto Nazionale di Fisica Nucleare, Pisa, Italy
e-mail: angela.bonaccorso@df.unipi.it

I. Tanihata et al. (eds.), *Handbook of Nuclear Physics*,
https://doi.org/10.1007/978-981-15-8818-1_3-1

Introduction

Direct nuclear reactions occur in a characteristic time of 10^{-22} s, the time it takes a nucleon to cross the nucleus. The short time only allows for the interaction with one or a few nucleons on the surface of the nuclei involved. Contrary to compound nucleus products, the direct reaction products are not distributed isotropically, but are focused in the forward direction. Bethe et al. (1952) first understood the mechanism of direct reactions as due mainly to a surface diffractive effect and showed the way to use them as spectroscopic tools. A recommended list of references, which will help the reader of this short and scope-limited review, is (Fesbach 1992; Satchler 1983; Broglia and Winther 1991; Bertulani and Danielewicz 2004; Canto and Hussein 2013). The dawn of direct reaction theory and its use to study nuclear structure has been recently reviewed in (Bonaccorso 2018).

Elastic Scattering

Upon hitting a target nucleus, the wave function of an impinging nucleus is modified by the scattering potential (For simplicity we assume a spherically symmetric potential.) $U(r)$, leading to the appearance of a phase shift of the outgoing part of the scattered wave. *Elastic scattering* occurs when there is no final energy transfer to the target nucleus. Generally, the projectile wave function is not only modified by a phase factor, but its magnitude might also change due to a loss of flux from the elastic channel. For a projectile with momentum $p = \hbar k$, the total wave function at a distance r from the scattering center is asymptotically given by

$$\Psi \to \frac{1}{2i}\sum_{\ell=0}^{\infty}(2\ell+1)i^l P_\ell(\cos\theta)\frac{S_\ell e^{i(kr-\ell\pi/2)} - e^{-i(kr-\ell\pi/2)}}{kr}, \tag{1}$$

where θ is the scattering angle and a sum is carried out for all *partial waves* (or quantized angular momenta) $\ell = 0, 1, 2, \cdots$. The complex coefficient S_ℓ is known as *scattering matrix*, or simply S-matrix. It is called a matrix because when more than one reaction possibility (or *reaction channel*) is available, the complex coefficient S_ℓ may acquire multiple labels. If $S_\ell = 1$, the sum in Eq. (1) leads to $\Psi \sim \exp(i\mathbf{k}.\mathbf{r})$, that is, a plane wave. But if

$$S_\ell = \exp[2i\delta_\ell], \tag{2}$$

and δ_ℓ is real, the incoming and outgoing waves have the same magnitude, and the scattering is termed *elastic*. The quantities δ_l are known as *phase shifts*.

The *partial wave expansion*, with the labels $\ell = 0, 1, 2, \cdots$ = (s, p, d, $\cdots$ waves), includes each of the angular momentum components ℓ (in units of $\hbar$) of the scattered wave. In classical mechanics, the angular momentum is given by $\ell = kb$,

where b is the *impact parameter*, i.e., the perpendicular distance to the target if the projectile would move along a straight line. But in quantum mechanics, ℓ is not a continuous variable, varying in steps of one. To determine the phase shifts and consequently the full scattering wave, one solves the Schrödinger equation (SE) for a given partial wave ℓ and its component m along the incident direction. For a spherically symmetric potential, one can write $\Psi_{\ell m} = Y_{\ell m}(\hat{\mathbf{r}})u_\ell(r)/(kr)$ where $Y_{\ell m}$ is a spherical harmonics function. One obtains

$$-\frac{\hbar^2}{2\mu}\left[\frac{d^2}{dr^2} - \frac{\ell(\ell+1)}{r^2}\right]u_\ell(r) + U(r)u_\ell(r) = Eu_\ell(r), \tag{3}$$

where μ denotes the reduced mass of the system. The numerical solution of this equation determines the modification of the partial wave u_ℓ with energy E from an undisturbed partial wave component of the plane wave. By matching the solution at large distances with the asymptotic plane-wave component, the phase shift is determined. For charged particles, the Coulomb potential U_C leads to an analytical solution of Eq. (3), and the phase shift is obtained by matching the solution for $U = U_N + U_C$, with the asymptotic Coulomb wave, where we denote U_N as the short-range part (nuclear) of the potential.

Adding all partial waves, Eq. (1) can be rewritten as a sum of a plane wave and a scattering outgoing wave, $\Psi \sim \exp(i\mathbf{k}.\mathbf{r}) + f(\theta)e^{ikr}/r$, with $f(\theta)$ accounting for the distortion of its outgoing part at the scattering angle θ. $f(\theta)$ is known as the *scattering amplitude*:

$$f(\theta) = \frac{1}{2ik}\sum_{\ell=0}^{\infty}(2\ell+1)(S_\ell - 1)P_\ell(\cos\theta). \tag{4}$$

The *differential scattering cross section* is obtained counting the number of particles scattered through an angle θ. This is achieved by calculating the particle current from the SE associated with the wave function Ψ. One obtains

$$\frac{d\sigma_e}{d\Omega} = |f(\theta)|^2 = \frac{1}{4k^2}\left|\sum_{\ell=0}^{\infty}(2\ell+1)(1 - S_\ell)P_\ell(\cos\theta)\right|^2. \tag{5}$$

The total scattering cross section is obtained by an integration over angles, yielding

$$\sigma_e = \pi\lambda\!\!\!^{-2}\sum_{\ell=0}^{\infty}(2\ell+1)|1 - S_\ell|^2, \tag{6}$$

with $\lambda\!\!\!^{-} = \lambda/2\pi = 1/k$. This method works for potentials that decay faster than $1/r$, or short-range potentials. For the Coulomb potential, the scattering amplitude becomes

$$f_C(\theta) = -\frac{\eta}{2k\sin^2(\theta/2)} e^{-i\eta \ln(\sin^2\theta/2)} e^{2i\sigma_0}, \tag{7}$$

where $\eta = Z_1 Z_2 e^2/\hbar v$ is the *Sommerfeld parameter*, with Z_1 and Z_2 being the nuclear charges and v their relative velocity, and $\sigma_0 = \arg\Gamma(1+i\eta)$ is the *Coulomb phase*. When the scattering occurs under the influence of short-range plus Coulomb potentials, the correct amplitude entering Eq. (5) is

$$f(\theta) = f_C(\theta) + f_N(\theta), \tag{8}$$

where f_N is the amplitude due to the short-range potential only.

In the presence of more than one channel, the elastic scattering may be influenced by the coupling between them, requiring the solution of coupled differential equations involving interactions between the channels, after which the S-matrices can be computed and the prescription leading to the Eq. (4) can be used. Some of the channels can be *inelastic*, absorbing energy and thus influencing the elastic scattering channel. Often, the number of channels is too many to be treated individually, and one introduces the concept of a complex *optical potential* (OP), U_{OP}, the imaginary part of which being responsible for the absorption into the inelastic channels. The elastic cross section is still given by Eq. (6), but the magnitude of the S-matrices for the elastic channel becomes smaller than unity. The absorption, or *reaction cross section*, σ_r, is given by

$$\sigma_r = \pi\lambda\!\!\!^{-2} \sum_{\ell=0}^{\infty} (2\ell+1)\left[1 - |S_\ell|^2\right]. \tag{9}$$

This equation has a simple interpretation. $\pi\lambda\!\!\!^{-2}$ is the "quantum area" for a projectile with momentum $k = 1/\lambda\!\!\!^{-}$, $2\ell+1$ is the number of magnetic states for an angular momentum ℓ, and $1 - |S_\ell|^2$ is the absorption probability for the partial wave ℓ.

In a different formalism, the scattering amplitude can be written as

$$f(\theta) = -\frac{\mu}{2\pi\hbar^2}\left\langle \mathbf{k}'|U|\psi_{\mathbf{k}}^{(+)}\right\rangle = -\frac{\mu}{2\pi\hbar^2} T(\mathbf{k}', \mathbf{k}), \tag{10}$$

where $\left|\mathbf{k}'\right\rangle$ is a Dirac "ket" notation for a plane wave with momentum $\mathbf{k}'$ and $\left|\psi_{\mathbf{k}}^{(+)}\right\rangle$ is the outgoing wave with momentum $\mathbf{k}$. $T(\mathbf{k}', \mathbf{k})$ is known as the *transition or T-matrix,* where

$$\left\langle \mathbf{k}'|U|\psi_{\mathbf{k}}^{(+)}\right\rangle = \left\langle \mathbf{k}'|T|\mathbf{k}\right\rangle = T(\mathbf{k}', \mathbf{k}). \tag{11}$$

A formal solution of the scattering problem requires the knowledge of the T-matrix. This can be achieved by iteration of the full Schrödinger equation, writing it in an operator form so that $H\psi = E\psi$. For positive energies E, ψ is the scattering wave

function. $H = H_0 + U$ is the Hamiltonian, with H_0 being here the kinetic energy operator $-\hbar^2\nabla^2/2\mu$. The formal solution for the T-matrix, entering Eq. (11), is

$$T = U + UG_0T = U + UG_0U + \cdots, \tag{12}$$

known as the *Lippmann-Schwinger (LS) equation*, where the so-called Green's function operator is defined as $G_0 = (H_0 - E)^{-1}$. The LS equation can be solved by iteration, as is indicated by the r.h.s. of (12). At high energies, an approximate solution of the Schrödinger equation yields the *eikonal phase shift* (Glauber 1959)

$$2\delta(b) = -\frac{1}{\hbar v}\int U_{OP}(r)dz, \tag{13}$$

where the radial coordinate describing the projectile-target relative motion is split into a transverse, **b**, and a longitudinal component, z, so that $\mathbf{r} \equiv (\mathbf{b}, z)$. The coordinate **b** is often interpreted as the impact parameter variable in classical mechanics. In the high-energy regime, the sum over partial waves in Eq. (4) involves too many terms. One can approximate the sum by an integral over b using $\ell = kb$ as a continuous variable. This procedure yields the simple formula (Glauber 1959)

$$f(\theta) = ik\int db\, b\, J_0(qb)\,[1 - S(b)]\,, \tag{14}$$

where $q = 2k\sin(\theta/2)$ is the *momentum transfer* in the collision, with the S-matrix given by $S(b) = \exp[2i\delta(b)]$ in the eikonal form. Again, for *multichannel reactions*, one needs to solve coupled-channels equations.

At low energies and/or in reactions involving highly charged nuclei, the elastic scattering is predominantly a *Coulomb scattering*. The differential scattering cross section is given by the *Rutherford formula*, $d\sigma_R/d\theta = a^4/\sin^4(\theta/2)$ with $a = Z_1Z_2e^2/\mu v^2$. A rough visualization of the scattering process assumes that the incoming wave splits into two pieces, one passing by one side and the other passing by the opposite side of the target (conveniently called the *near* and *far sides*). When these two pieces do not interfere, one recovers the *classical scattering*. A good measure of the passage from the classical to quantum scattering regime is obtained by using the *Sommerfeld parameter* $\eta = Z_1Z_2e^2/\hbar v$. When η decreases, the scattering is increasingly influenced by the interference of the near- and the far-side waves. Around $\eta \sim 10$ the scattering changes from the so-called *Fresnel* to the *Fraunhofer* regime. This is clearly seen in Fig. 1.

It is clearly visible on the left panel of Fig. 1 that the elastic scattering in the Fraunhofer regime displays wiggles that are nearly equally displaced. The distance between the dips in the angular distribution is telltales of the size R of the system involved, i.e., $\Delta\theta \sim 1/kR$, whereas the nearly exponential falloff of the cross section is due to the diffuseness a of the nuclear surface, i.e., $\sigma(\theta) \propto \exp(-qa)$, with q being the momentum transfer defined previously. Therefore, elastic scattering is a very good probe of the *nuclear geometry* of the optical potential. Figure 2 shows

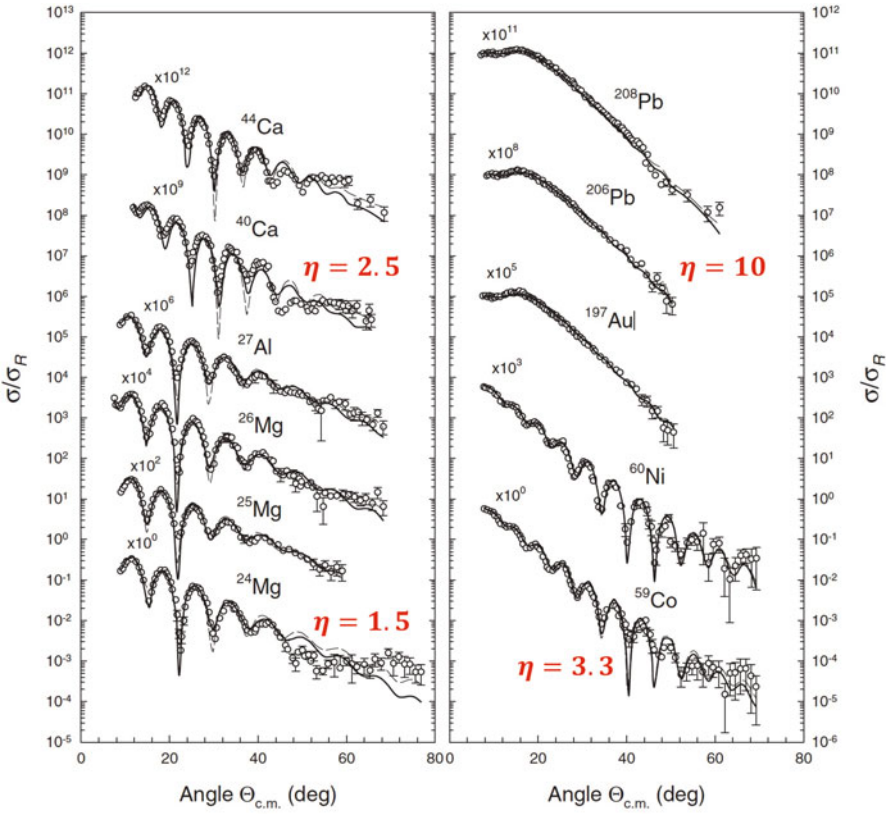

Fig. 1 Ratio between the measured cross sections and the Rutherford scattering cross sections for ^{6}Li projectiles incident on different targets at 88 MeV. One clearly sees the transition from classical to quantum scattering as the Sommerfeld parameter η decreases. Full quantum interference is visible for very small values of η (Fraunhofer scattering). (Adapted from Ref. Hossain et al. 2013)

examples of elastic scattering angular distributions of ^{9,10,11}Be + Pb at 140 MeV (about 3.5 times the Coulomb barrier) (Duan et al. 2020). It also shows how the scattering angle pattern of elastic scattering for a large value of η spreads to larger angles as the mass of the projectile decreases. But also of relevance for this pattern is the role of the weakly bound nucleons, to be discussed later.

Inelastic Scattering

Inelastic scattering occurs when a state in the projectile or target nucleus is excited in the reaction. Consider a nucleus in an initial state $|\, i\rangle$ as an eigenstate of the internal nuclear Hamiltonian H_0. In a direct reaction, the nucleus will be subject

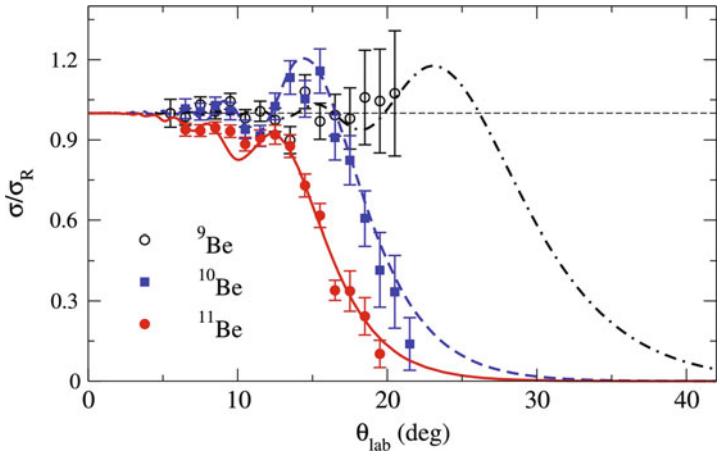

Fig. 2 Examples of elastic scattering angular distributions of ^{9,10,11}Be + Pb at 140 MeV (about 3.5 times the Coulomb barrier). Adapted from Ref. (Duan et al. 2020)

to an interaction potential U with another nucleus (or with a nucleon). If this interaction can be treated perturbatively, *Fermi's Golden rule* can be used to obtain the cross section for the excitation of a final state $|\ f\rangle$, i.e.,

$$\sigma = \frac{\mu}{\hbar k}\frac{2\pi}{\hbar}\,|\langle f|U|i\rangle|^2\,\rho(E_f), \tag{15}$$

where ρ is the *density of the final states*, i.e., the number of states per energy interval at the final energy E_f. The nuclear wave functions $|i,\ f\rangle$ include the internal wave function $|\phi\rangle$ of the excited nucleus as well as the relative motion wave function, $|\ \chi\rangle$.

The "bra" and "ket" notation used in the above relation can be rewritten in terms of the *intrinsic nuclear coordinate*, $\mathbf{x}$, and the *relative motion coordinate* $\mathbf{y}$,

$$\sigma = \frac{2\pi\mu}{\hbar^2 k}\rho(E_f)\left|\int d^3x d^3y \phi_f^*(\mathbf{x})\chi^{(-)*}(\mathbf{y})U(\mathbf{x},\mathbf{y})\phi_i(\mathbf{x})\chi^{(+)}(\mathbf{y})\right|^2, \tag{16}$$

where the notation $\chi^{\pm}$ stands for outgoing (incoming) relative motion wave function. In the *plane-wave Born approximation* (PWBA), the wave functions χ are taken as plane waves, and the integral above becomes a Fourier transform for the momentum transfer $\mathbf{q} = \mathbf{k}' - \mathbf{k}$. But, the relative motion wave function χ can be calculated exactly by solving the SE for the scattering part separately, with the proper energies E_i and E_f and optical potentials V_1 and V_2 for the incoming and outgoing channel, respectively. In this case, Eq. (16) is known as the *distorted-wave Born approximation* (DWBA). Figure 3 shows schematically that the terminology "Born" in the DWBA means that the perturbation theory is treated to first-order only, i.e., the excited nucleus is assumed to interact only once and weakly with the

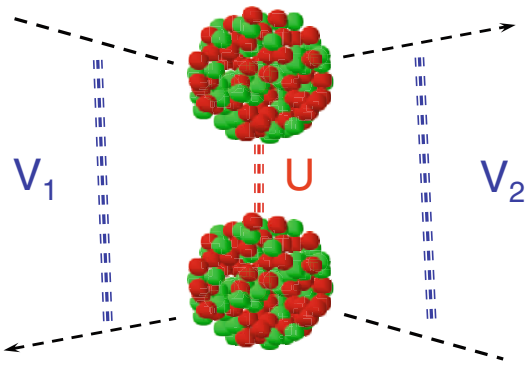

Fig. 3 Schematic representation of inelastic scattering described within DWBA. The nuclear interaction is taken to first order (the B in DWBA), and the distorted waves are calculated exactly given the entrance, V_1, and outgoing channel, V_2, optical potentials

other nucleus, while "distorted" means that the relative motion between the nuclei in the entrance and the outgoing channels is taken into account to all orders.

Angular distributions for inelastic scattering display similar features as elastic scattering such as oscillations, with the distance between dips becoming a telltale of the geometry of the reacting nuclei. However, in contrast to elastic scattering and due to the presence of the interaction potential U in Eq. (16), inelastic scattering data do not often display an exponential falloff at the Fraunhofer regime because of the diffuseness of the nuclear densities. The details of the inelastic cross section will contain information of $U(\mathbf{r})$, as well as the internal wave functions ϕ. If the optical potential (determining the distorted waves) and the interaction potential (responsible for the excitation) are both well known, inelastic scattering can be used as a tool for spectroscopic studies of the internal wave function ϕ.

Coupled Channels

The Schrödinger equation (SE) of a nuclear system subject to an external agent $V(t)$ is governed by the Hamiltonian $H(t) = H_0 + V(t)$ where H_0 is the non-perturbed Hamiltonian H_0. Let us assume that H_0 has eigenvalue and eigenfunction solutions, i.e., that $H_0\psi_n(\mathbf{r}) = E_n\psi_n(\mathbf{r})$, and that the eigenfunctions ψ_n form a complete basis. The total wave function Ψ, obeying the time-dependent SE, $H\Psi = i\hbar\partial\Psi/\partial t$, may be expanded as $\Psi = \sum_n a_n(t)\psi_n e^{-iE_nt/\hbar}$, where a_n are time-dependent coefficients. Inserting this expansion into the time-dependent SE leads to

$$i\hbar\sum_n \dot{a}_n\psi_n e^{-iE_nt/\hbar} = \sum_n V a_n\psi_n e^{-iE_nt/\hbar}, \tag{17}$$

with $\dot{a}_n \equiv da_n(t)/dt$. From the orthogonalization properties of the ψ_n, multiplying (17) by ψ_k^* and integrating it over the $\mathbf{r}$, one obtains the *time-dependent coupled-channels* equations

$$\dot{a}_k\,(t) = -\frac{i}{\hbar}\sum_n a_n\,(t)\;\; V_{kn}\,(t)\;\; e^{i\,\frac{E_k - E_n}{\hbar}t}, \tag{18}$$

where $V_{kn} = \int \psi_k^* V \psi_n \, d^3r$.

A simple derivation of the *time-independent coupled-channels equations* can be achieved for high-energy collisions. The replacement $z = vt$ can be done for an almost undisturbed trajectory of a projectile with velocity v passing by the target nucleus with an impact parameter b. The general coupled equations are then simply an outcome of Eq. (18), i.e., Bertulani (2005)

$$i\hbar v \frac{d}{dz}\mathscr{A}_c(b,z) = \sum_{c'} \langle \Psi_c | V_{int}(b,z) | \Psi_{c'} \rangle \; \mathscr{A}_{c'}(b,z)\; e^{iE_{cc'}z/v}, \tag{19}$$

where we introduced the channel index $c = \{i, \ell, m\}$, with i denoting one of the nuclear states $i > 0$, $i = 0$ the ground state, and ℓ and m are the orbital angular momentum and its projection along the incident z-axis. $E_{cc'} = E_{c'} - E_c$ is the excitation energy. The amplitudes a_c were renamed to $\mathscr{A}_c(b,z)$. By solving these equations, using the initial condition, $\mathscr{A}_c(b,-\infty) = \delta_{c0}$, one can obtain the probability that a channel c is populated in the reaction, $|\mathscr{A}_c(b,\infty)|^2$.

At lower energies, where the partial wave expansion is more adequate, one can easily deduce the corresponding coupled-channels equations from Eq. (19) by using the correspondence of the continuous variable b with the angular momentum: (To be more precise, one should use $b \to (\ell+1/2)/k$.) $b \to \ell/k$. The integrals over the impact parameter become a sum over the partial waves ℓ. Finally, the consideration of total angular momenta and spin coupling can be accounted for, with channels discerning by the angular momentum quantum numbers (J, M).

At high energies, the angular distribution of the inelastically scattered particles for the excitation of the channel state c is obtained from

$$f_c^{\mu}(\theta) = ik \int_0^{\infty} dbbJ_{\mu}(qb)S(b)\mathscr{A}_c(b,\infty), \tag{20}$$

with k being the projectile wavenumber and $q = 2k\sin(\theta/2)$ the momentum transfer. Here, we simplified the notation using $\mu = M_c - M_0$, with M_i being the magnetic quantum number associated with the total angular momentum J_i. Averaging over the initial spin and summing over the final spin yields the differential cross section

$$\frac{d\sigma_c}{d\Omega} = \frac{1}{2J_0+1}\sum_{M_0,M_c}\left|f_c^{(M_c-M_0)}(\theta)\right|^2. \tag{21}$$

At high energies, the S-matrices in Eq. (20) are given by $S(b) = \exp\{2i\delta(b)\}$ where the phase shift can be related to the corresponding nucleon-nucleon (NN) scattering quantities (Hussein et al. 1991). In this case, the eikonal phase becomes

$$2\delta(b) = \int \rho_P(q)\Gamma(q)\rho_T(q)J_0(qb)q\,dq, \tag{22}$$

where J_0 is the ordinary Bessel function of zeroth order, and the nucleon-nucleon scattering profile function is parametrized as (Ray 1979)

$$\Gamma(q) = \frac{i+\alpha_{NN}}{4\pi}\sigma_{NN}e^{-\beta_{NN}q^2}. \tag{23}$$

σ_{NN} is the total nucleon-nucleon cross section, and α_{NN} is the ratio between the real and the imaginary part of the NN scattering amplitude. β_{NN} is a momentum dependence parameter. These parameters are fitted to reproduce the NN scattering observables. Tables with the energy dependence of these parameters are given in Refs. Hussein et al. (1991), Aumann and Bertulani (2020).

The total excitation cross section for channel c averaged over the initial spin J_0 is given by

$$\sigma_c = \frac{2\pi}{2J_0+1}\int dbb|S(b)|^2\,|\mathscr{A}_c(b,\infty)|^2\,. \tag{24}$$

The coupled-channels method can be used with any nuclear structure model, either from a two-body, three-body, or many-body description of the nucleus enabling the calculation of the matrix elements $\langle\Phi_c|V_{int}(b,z)|\Phi_{c'}\rangle$ in Eq. (19). *First-order excitation amplitudes* can be calculated from Eq. (19) replacing $\mathscr{A}_c(b,z) = \delta_{c0}$ on its right-hand side, leading to

$$\mathscr{A}_c(b,\infty) = -\frac{i}{\hbar v}\int_{-\infty}^{\infty} dz\,\langle\Phi_c|V_{int}(b,z)|\Phi_0\rangle\;\; e^{iE_{0c}z/v}. \tag{25}$$

If the states c are in the continuum, then Eq. (21) means

$$\frac{d\sigma_c}{d\Omega dE} = \frac{1}{2J_0+1}\sum_{M_0,M_c}\left|f^{(Mc-M_0)}(\theta,\,E=E_c)\right|^2, \tag{26}$$

for one of the states in the continuum with energy E_c.

The angular distribution integrated over all continuum energies is given by

$$\frac{d\sigma_c}{d\Omega} = \frac{1}{2J_0+1}\sum_{M_0,M_c}\int dE\left|f^{(Mc-M_0)}(\theta,\,E)\right|^2. \tag{27}$$

For large bombarding energies so that $q \simeq k\theta \simeq k\sin\theta$, it follows that $d\Omega = 2\pi q dq/k^2$, and

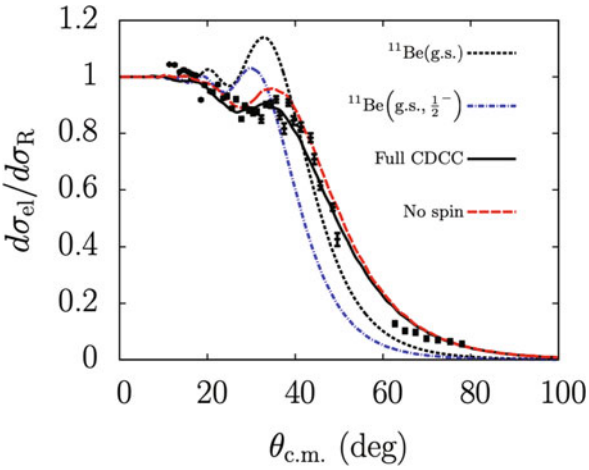

Fig. 4 CDCC calculations (Druet and Descouvemont 2012) for ^{11}Be + ^{64}Zn at 24.5 MeV compared to experimental data (Di Pietro et al. 2010). ^{11}Be(g.s.) and ^{11}Be(g.s., $1/2^-$) denote the one-channel (ground state only) and two-channel calculations (ground state and the first excited state). The elastic cross sections are divided by the Rutherford cross sections. Calculations based on CDCC, shown as a continuous curve, nearly match the data, taking into account a discretized continuum. The long-dashed curve neglects the spin of the projectile

$$\sigma_c = \frac{2\pi}{2J_0+1}\sum_{M_0,M_c}\int dbb\int db'b'\int dqq\,J_\mu(qb)J_\mu(qb')S(b)S^*(b')$$
$$\times\mathscr{A}(b,\infty)\mathscr{A}^*(b',\infty) = \frac{1}{2J_0+1}\int db\,b|S(b)|^2\,|\mathscr{A}_c(b.\infty)|^2\,. \quad (28)$$

In calculations involving weakly bound nuclei, the transition to the continuum (breakup) is followed by a coupling between states in the continuum. The states in the continuum can be treated as isolated *discretized states*. Such formalism is known as the *continuum-discretized coupled-channels* (CDCC) equations. Figure 4 shows an example of a coupled-channels calculation with the addition of couplings in the continuum (Druet and Descouvemont 2012). One sees that the inclusion of channel coupling considerably improves the comparison with the experiment (Di Pietro et al. 2010). Due to the relatively low energy of the projectile (24.5 MeV), the CDCC calculations are in this case performed using the partial wave expansion method.

The Optical Potential

The simple description of high-energy collisions presented above is not adequate at lower energies, and a good knowledge of an *optical potential* U will be the most important ingredient in the calculations of elastic and inelastic scattering. The optical potential (OP) contains information about the leakage of probability

from a channel of interest, e.g., the elastic channel, to other channels involving the excitation of nuclear states. Traditional theoretical methods assume that all our ignorance about the numerous relevant channels can be simulated by the introduction of an imaginary potential W. A popular form of the *phenomenological OP* is

$$U(r) = V_0(r) + V_s(r)(\mathbf{l}\cdot\mathbf{s}) + V_C(r) + iW(r), \tag{29}$$

where V_0 is the *central part* of a real potential, V_s is a *spin-orbit component*, and V_C is the *Coulomb potential* between the nuclei. The functional forms of the potentials V_0 and W are usually taken as a *Woods-Saxon (or Fermi) function*

$$f(r) = \frac{f_0}{1+\exp\left(\frac{r-R_0}{a_0}\right)}, \tag{30}$$

where f_0 (*strength*), R_0 (*radius*), and a_0 (*diffuseness*) are taken as adjustable parameters. The second term on the r.h.s. of Eq. (29) is usually taken as a derivative of the function (30) and accounts for the increased probability of nucleon-nucleon collisions at the nuclear surface due to a decrease of the *Pauli principle* at lower nucleon densities. It also accounts for the surface preference of the spin-orbit potential.

Many other methods exist to deduce the optical potential from basic details of nuclear structure and reactions. A popular case is the *folding potential*, obtained from the ground-state nuclear densities $\rho(\mathbf{r})$ and the nucleon-nucleon potential

$$\begin{aligned} U(\mathbf{r}) &= \int d^3r' v_{NN}(\mathbf{r}'-\mathbf{r})\rho_A(\mathbf{r}'), \quad \text{for nucleon-nucleus,} \\ &= \int d^3r' v_{NN}(\mathbf{r}'+\mathbf{r}''-\mathbf{r})\rho_A(\mathbf{r}')\rho_B(\mathbf{r}''). \quad \text{for nucleus-nucleus.} \end{aligned} \tag{31}$$

To these real potentials, corresponding imaginary parts are introduced usually with the same form as the real parts multiplied by constants adjusted to reproduce experimental observables. A modification of these equations can be introduced to account for *medium effects* of the nucleon-nucleon interaction, v_{NN}, inducing an energy dependence $v_{NN}(\mathbf{r}, E)$ to obtain a corresponding energy-dependent optical potential $U(\mathbf{r}, E)$. A variety of *effective interactions* accounting for medium effects have been developed such as the M3Y (Bertsch et al. 1977), Love-Franey (Franey and Love 1985), the JLM (Jeukenne et al. 1977), and many other popular optical potentials.

A *microscopic formalism* for the optical potential can be developed by linking the T-matrix for the nucleus-nucleus collisions to T-matrices for nucleon-nucleon scattering. As a starting point, one uses the Lippmann-Schwinger equation for the whole system of $A + B$ nucleons, yielding the approximate equation (Feshbach 1958)

$$U = \sum_{i \neq j} t_{ij} + \sum_{i \neq j} t_{ij} \frac{1 - |\Psi_0 >< \Psi_0|}{E + \hbar^2 \nabla^2 / 2\mu + i\varepsilon} t_{ij} + \cdots = U_{LO} + U_{NLO} + \cdots , \quad (32)$$

where the sum runs over all nucleons, E is the total energy of the colliding nucleus-nucleus system, t_{ij} are the T-matrices for (free) nucleon-nucleon scattering for their relative motion, ∇ is a derivative of the center-of-mass motion of the system, and $|\Psi_0\rangle = \left|\Psi_0^A\right\rangle \left|\Psi_0^B\right\rangle$ is the product of the ground-state wave functions for nuclei A and B. The factor $i\varepsilon$ is included in Eq. (32) to account for the proper outgoing wave boundary condition. As shown in Ref. (Hussein et al. 1991), this formalism allows for an understanding on how the optical potential is influenced by multiple nucleon-nucleon collisions, where U_{LO} is the *leading-order* optical potential, U_{NLO} the *next-to-leading order* correction, and so on. For heavy nuclei, U_{NLO} and higher-order corrections still comprise an important part of the whole optical potential (Hussein et al. 1991).

The medium effects on the nucleon-nucleon scattering cannot be neglected in most cases. Introducing the Pauli principle for nucleon-nucleon scattering in the medium implies solving an equation similar to the Lippmann-Schwinger equation, known as the *G-matrix*, and often written the form of the *Bethe-Goldstone equation* (Gomes et al. 1958)

$$\left\langle \mathbf{k}' | G | \mathbf{k} \right\rangle = \left\langle \mathbf{k}' | v_{NN} | \mathbf{k} \right\rangle + \int \frac{d^3 k''}{(2\pi)^3} \frac{\left\langle \mathbf{k}' | v_{NN} | \mathbf{k}'' \right\rangle Q(\mathbf{k}'') \left\langle \mathbf{k}'' | G | \mathbf{k} \right\rangle}{E(\mathbf{P}'', \mathbf{k}'') - E_0 + i\varepsilon}, \quad (33)$$

where $E(\mathbf{P}, \mathbf{k}) = e(\mathbf{P} + \mathbf{k}) + e(\mathbf{P} - \mathbf{k})$ are off-shell nucleon single-particle energies, with $\mathbf{P}$ being the nucleon-nucleon center-of-mass momentum and $\mathbf{k}$ their relative momentum. E_0 is the on-shell energy, i.e., when the final and initial energies and momenta of the nucleons obey conservation laws. As with the case of the Lippmann-Schwinger equation, the Bethe-Goldstone equation can be solved by iteration. The operator $Q(\mathbf{k}'')$ is equal to one if the individual momenta of the nucleons are larger than the local Fermi momentum, i.e., if $|\mathbf{k}_{1,2}| > k_F$, where $\mathbf{k}_{1,2} = \mathbf{P} \pm \mathbf{k}$. If this condition is not valid, $Q(\mathbf{k}'') = 0$.

A similar method accounts for the medium modification of the nucleon-nucleon force and is known as the *Brueckner theory*. Similar to the Bethe-Goldstone equation, the nucleon-nucleon interaction in the nuclear medium is formally given by Goldstone (1957)

$$v(p) = \langle p | v | p \rangle = Re \sum_{k < k_F} \langle pq | G | pq - qp \rangle , \quad (34)$$

where $|pq - qp\rangle$ is a short-hand notation of the anti-symmetrization of the nucleon wave functions. In the Brueckner scheme, this equation is solved self-consistently, i.e., the single-particle energies e depend on the nucleon-nucleon potential $v(p)$, which depends on the solution for the G-matrix, which in turn depends on e and $v(p)$.

A microscopic description of the optical potential has to include the loss of energy into nuclear excitation and the details of the nuclear wave functions. A traditional method to tackle these features uses the concept of *self-energies* induced by all possible intermediate states. For example, in the particle-vibrator coupling model (Bernard and Van Giai 1980), the optical potential arises from the relation

$$U(E, \mathbf{r}, \mathbf{r}') = U_{HF}(\mathbf{r}, \mathbf{r}') + \Sigma(E, \mathbf{r}, \mathbf{r}'), \tag{35}$$

where U_{HF} is a *mean-field potential* and the self-energy is given by

$$\Sigma(E, \mathbf{r}, \mathbf{r}') = \frac{1}{2J_0 + 1} \left(\sum_{nL, p>F} \frac{|\langle i||V||p, nL\rangle|^2}{E - \varepsilon_p - E_{nL} - i\eta} + \sum_{nL, h<F} \frac{|\langle i||V||h, nL\rangle|^2}{E - \varepsilon_h + E_{nL} - i\eta} \right), \tag{36}$$

with $|nL>$ denoting phonon states, $|p\rangle$ ($|h\rangle$) particle (hole) states, and ε_p (ε_h) their respective energies. A nuclear structure model is used to obtain the wave functions corresponding to all the states entering this equation.

There exist other microscopic formalisms for the optical potentials such as the *dispersive optical potential model* (DOM) based on its functional analytical properties (Mahaux and Sartor 1991). It recalls the physical concept that a scattered wave is only emitted after the arrival of the incident wave. As a consequence, one finds that

$$U(E, \mathbf{r}, \mathbf{r}') = U_0(\mathbf{r}, \mathbf{r}') + V(E, \mathbf{r}, \mathbf{r}') + iW(E, \mathbf{r}, \mathbf{r}'), \tag{37}$$

where the real and imaginary parts of the potential are related by the *dispersion relation*

$$W(E, \mathbf{r}, \mathbf{r}') = i\frac{\mathscr{P}}{\pi} \int dE' \frac{V(E, \mathbf{r}, \mathbf{r}')}{E - E'}, \tag{38}$$

where $\mathscr{P}$ denotes the principal value of the integral. The DOM has been applied to a large number of data (see, e.g., Ref. Mueller et al. 2011), and microscopic *ab initio calculations* for the nuclear states have been incorporated in its numerical derivation (Waldecker et al. 2011).

Coulomb Excitation

Coulomb excitation is a specific inelastic scattering process where one nucleus excites another via its electromagnetic (EM) field V. The EM field can be decomposed in a sum of multipoles, for example, $E1$, $E2$, $M1$, $\cdots$, each one containing angular momentum and parity. At low-collision energies, $E2$ (electric quadrupole) excitations are stronger, whereas at higher energies $E1$ (electric dipole) excitations prevail.

At low energies (below the Coulomb barrier), Coulomb excitation has been used to analyze experiments on multiple excitations and reorientation effects (Alder and Winther 1965; Cline 1986). At relativistic energies, the kinematics is characterized by near straight-line trajectories and by retardation effects due to special relativity (Alder and Winther 1975). A full quantum mechanical theory of relativistic Coulomb excitation was developed in Refs. Bertulani and Baur (1985), Bertulani and Nathan (1993), including diffraction and absorptive effects. At intermediate energies ($20 < E_{lab} < 200$ MeV/nucleon), both retardation and relativistic corrections of the Rutherford trajectories are necessary for an accurate description of the reaction (Aleixo and Bertulani 1989).

In first-order perturbation theory, the differential cross section is given by

$$\frac{d\sigma_{i\to f}}{d\Omega} = \frac{d\sigma_R}{d\Omega}\frac{16\pi^2 Z_2^2 e^2}{\hbar^2}\sum_{\pi\lambda\mu}\frac{B(\pi\lambda, I_i \to I_f)}{(2\lambda+1)^3} \mid S(\pi\lambda,\mu) \mid^2, \tag{39}$$

where $d\sigma_R/d\Omega$ is the Rutherford cross section and Z_2 is the projectile charge. $B(\pi\lambda, I_i \to I_f)$ is known as the *reduced matrix element* of the excited nucleus, where $\pi\lambda = E1,\ E2,\ M1, \ldots$ is the excitation multipolarity, and $\mu = -\lambda, -\lambda+1, \ldots, \lambda$. The *orbital integrals* $S(\pi\lambda,\mu)$ include information on the reaction dynamics, i.e., on the details of the EM fields (Aleixo and Bertulani 1989).

Coulomb excitation is an external process, occurring when the nuclear matter of the nuclei do not overlap. This implies that the Coulomb excitation matrix elements display the same form, or operators, as those for the excitation by real photons (except for $E0$ excitations, usually very small). As a consequence, the Coulomb excitation cross sections can always be written as (Bertulani and Baur 1988)

$$\frac{d\sigma_C\,(E_x)}{dE_x} = \sum_{E\lambda}\frac{n_{E\lambda}\,(E_x)}{E_x}\sigma^{\gamma}_{E\lambda}\,(E_x) + \sum_{M\lambda}\frac{n_{M\lambda}\,(E_x)}{E_x}\sigma^{\gamma}_{M\lambda}\,(E_x)\ , \tag{40}$$

where $\sigma^{\gamma}_{\pi\lambda}\,(E_x)$ are *cross sections induced by real photons* (photonuclear cross sections) with multipolarity $\pi\lambda$. E_x is the excitation (or photon) energy, and $n_{M/E\lambda}(E_x)$ are known as *virtual photon numbers* (Bertulani and Baur 1988).

Photoabsorption cross sections are functions of the reduced matrix elements, for the excitation energy E_x. Explicitly (Bertulani and Baur 1988),

$$\sigma^{\pi\lambda}_{\gamma}(E_x) = \frac{(2\pi)^3(\lambda+1)}{\lambda\,[(2\lambda+1)!!]^2}\left(\frac{E_x}{\hbar c}\right)^{2\lambda-1}\frac{dB\,(\pi\lambda, E_x)}{dE_x}, \tag{41}$$

where dB/dE_x are known as *electromagnetic response functions*. The *total transition strength* is the integral

$$B(\pi\lambda, I_i \to I_f) = \int dE_x\ \frac{dB\,(\pi\lambda, E_x)}{dE_x}. \tag{42}$$

The differential cross sections can also be expressed in terms of equivalent photons, namely,

$$\frac{d\sigma_C(E_x)}{d\Omega} = \frac{1}{E_x}\sum_{\pi\lambda}\frac{dn_{\pi\lambda}}{d\Omega}(E_x,\theta)\sigma_\gamma^{\pi\lambda}(E_x), \tag{43}$$

with Ω being the solid scattering angle. This is the same as Eq. (39), but rewritten in a simpler form, helping us to immediately see the connection with the cross sections induced by real photons.

Figure 5 shows a calculation ($E_\gamma \equiv E_x$) for virtual photons with $E1$ multipolarity, and three typical bombarding energies, "as viewed" by a lead projectile incident on a lead target at impact parameters larger than $b = 12.3$ fm. When the projectile energy increases, more virtual photons with larger energies become available. The energy of states probed is also increased, making it possible to study giant resonances, lepton and meson production, and the production of heavy particles (Bertulani and Baur 1988).

A photonuclear reaction can access information complementary to Coulomb excitation. For photon energies larger than nucleon separation energies, the photoabsorption cross section displays characteristic single-particle resonances. For energies in the range of 15–25 MeV, a wide and large peak is observed, known as the *giant electric dipole resonance* ($E1$ excitation). Figure 6 exhibits the photoabsorption cross section of ^{136}Xe at photon energies around the electric dipole giant resonance and the double giant dipole resonance (Schmidt et al. 1993).

Giant resonances occur in basically all nuclei along the periodic table. Their centroid energy decreases following the phenomenological formula $E_{GDR} \simeq 80/A^{1/3}$ for $A > 20$. Their widths are almost all in the range between 3.5 MeV and 5 MeV, with few cases reaching up to 7 MeV. They are collective excitations with many nucleons participating at once. The oscillating electric field of a photon effectively induces collective oscillations of protons against neutrons. Among the giant resonances, the *giant electric dipole (GDR) resonance* absorbs one unit of

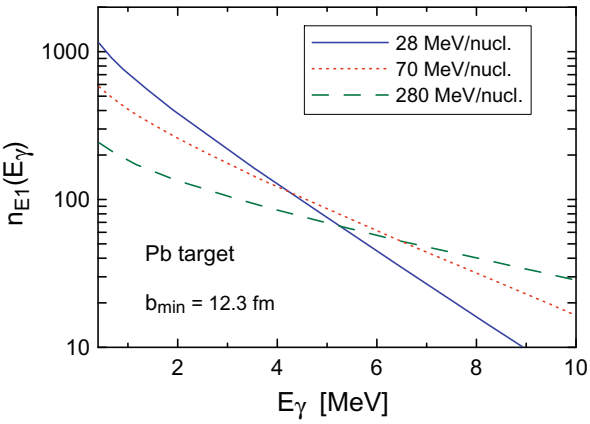

Fig. 5 Number of virtual photons with $E1$ multipolarity, for three typical bombarding energies, "as viewed" by a Pb projectile nucleus incident on a Pb target with impact parameters larger than $b_{min} = 12.3$ fm

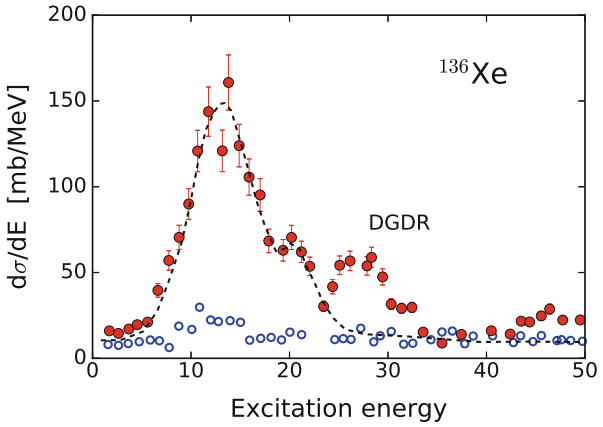

Fig. 6 Coulomb excitation cross section for ^{136}Xe (700 MeV/nucleon) nuclei impinging on lead (solid circles) and carbon nuclear targets (open circles). The dashed curve includes the excitation of isoscalar and isovector giant quadrupole resonances and the isovector giant dipole resonance (IVGDR). The double giant dipole resonance (DGDR) was clearly identified as a bump in the spectrum at about twice the energy of the IVGDR (Schmidt et al. 1993)

angular momentum ($\Delta l = 1$), e.g., if the nucleus is even-even, it is taken to an 1^- state. It is also an *isovector resonance* because isospin is also changed by one unit ($\Delta T = 1$). Protons and neutrons vibrating in phase yield *isoscalar resonances* ($\Delta T = 0$), and if in opposite phases, they yield *isovector resonances* ($\Delta T = 1$). The photon excites less effectively giant isoscalar resonances, with $\Delta T = 0$. Isoscalar monopole ($\Delta l = 0$) resonances are mostly excited in reactions involving the nuclear interaction. In a *giant electric quadrupole resonance*, the nucleus vibrates in an ellipsoidal mode. In a giant monopole resonance, the nucleus contracts and expands radially, known as a *breathing mode*, also occurring in isoscalar and isovector forms. Monopole resonances are a good probe of the *compressibility of nuclear matter*.

Magnetic giant resonances involve *spin vibrations* where nucleons with spin-up oscillate out of phase with nucleons with spin-down, also including isoscalar and isovector modes. Charge-exchange reactions are a good probe of magnetic resonances induced when a projectile charge changes down to $Z - 1$ or up to $Z + 1$, as, for example, induced in (p,n), (d,p), and (d,n) reactions. Giant spin-flip resonances are also known as *giant Gamow-Teller resonances*.

Giant resonances have also been observed in excited nuclei, first predicted by using the Brink-Axel hypothesis (Brink 1955; Axel 1962). Two giant resonances can be excited simultaneously, e.g., the double giant dipole resonance (or *multiphonon giant resonance*) has been observed in double charge-exchange reactions with pion probes in ^{32}S (Mordechai et al. 1988). Coulomb excitation is perhaps the best probe to excite giant multiphonon resonances, as predicted in Ref. (Bertulani and Baur 1988) and observed in Ref. (Schmidt et al. 1993). Figure 6 shows a beautiful example of the excitation of the double giant resonance.

Charge-Exchange Reactions

Charge-exchange reactions are used as a probe to extract the magnitude of *Gamow-Teller*, $B(GT)$, and *Fermi*, $B(F)$, *matrix elements*, not accessible in β-decay experiments (Taddeucci et al. 1987). This technique relies on the similarity of the interaction in charge-exchange reactions and the spin-isospin operators involved in weak decay. Using the DWBA approximation, one can show that the cross section for charge exchange at small momentum transfers q is proportional to $B(GT)$ and $B(F)$ (Bertulani 1993):

$$\frac{d\sigma}{d\Omega}(\theta = 0^\circ) = \left(\frac{\mu}{2\pi\hbar}\right)^2 \frac{k_f}{k_i} N_D |J_{\sigma\tau}|^2 \left[B(GT) + C_F B(F)\right], \tag{44}$$

where μ is the reduced mass, $k_i(k_f)$ is the initial (final) relative momentum, N_D is a correction factor (accounting for initial- and final-state interactions), $J_{\sigma\tau}$ is the volume integral of the GT part of the effective nucleon-nucleon interaction, the constant $C_F = |J_\tau/J_{\sigma\tau}|^2$ accounts for possible Fermi excitations, and $B(\alpha = GT, F)$ is the reduced transition probability for spin-flip and non-spin-flip transitions (τ_k is the isospin operator). For non-spin-flip transitions, it is given by

$$B(F) = \frac{1}{2J_i + 1} |\langle f || \sum_k \tau_k^{(\pm)} || i \rangle|^2,$$

and for spin-flip (σ_k is the spin operator),

$$B(GT) = \frac{1}{2J_i + 1} |\langle f || \sum_k \sigma_k \tau_k^{(\pm)} || i \rangle|^2.$$

Small momentum transfers, $q \sim 0$, occur at very small scattering angles, when $\theta \ll 1/kR$, where R is a rough measure of the nuclear radius and k is the projectile wavenumber.

Charge-exchange reactions at high energies are due to the exchange of charged pions and rho mesons carrying spin and isospin quantum numbers. Figure 7 displays the energy dependence of the nucleon-nucleon potential at forward angles. The separate contributions of spin-isospin, $\sigma\tau$, and isospin, τ, parts of the interaction are also shown. One observes that intermediate energy collisions, i.e., around $E \sim 100$–300 MeV, have larger $\sigma\tau$ than τ contributions. For this reason, this energy range is better suited for studies of the Gamow-Teller matrix elements needed for astrophysics. Therefore, at intermediate energy collisions,

$$\frac{d\sigma}{dq}(q = 0) \sim K N_D |J_{\sigma\tau}|^2 B(GT), \tag{45}$$

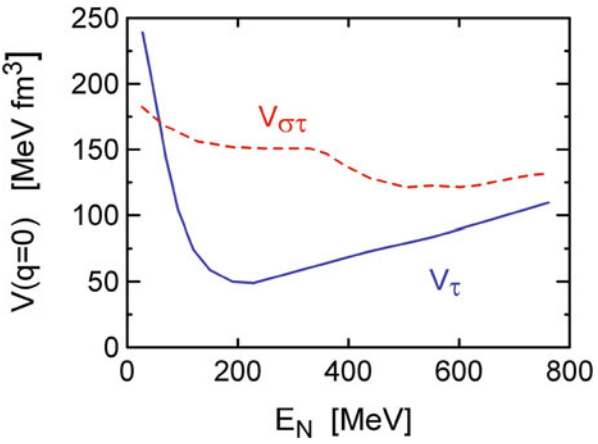

Fig. 7 Strength of the nucleon-nucleon potential at forward scattering angles. Separate contributions are shown for the spin-isospin, $\sigma\tau$, and the isospin, τ, components of the interaction as a function of the laboratory energy

with K being a kinematical constant. In the plane-wave Born approximation, the charge-exchange scattering matrix elements are given by Bertulani (1993)

$$\mathscr{M}_{exch}(\mathbf{q}) = \left\langle \Psi_A^{(f)}(\mathbf{r}_A)\Psi_B^{(f)}(\mathbf{r}_B) \left| e^{-i\mathbf{q}\cdot\mathbf{r}_A} V_{exch}(\mathbf{q}) e^{i\mathbf{q}\cdot\mathbf{r}_B} \right| \Psi_A^{(i)}(\mathbf{r}_A)\Psi_B^{(i)}(\mathbf{r}_B) \right\rangle, \tag{46}$$

with $\mathbf{q}$ being the momentum transfer and $\Psi_{A,B}^{(i,f)}$ the intrinsic wave functions of nuclei A and B for the initial i and final f states. $\mathbf{r}_{A,B}$ are intrinsic coordinates of the participating nucleons, and V_{exch} is charge-exchange part of the nucleon-nucleon interaction containing spin and isospin operators. At forward angles and low-momentum transfers, $\mathbf{q} \sim 0$, the matrix element (46) becomes

$$\mathscr{M}_{exch}(\mathbf{q} \sim 0) \sim V_{exch}^{(0)}(\mathbf{q} \sim 0)\, \mathscr{M}_A(F, GT)\, \mathscr{M}_B(F, GT)\,, \tag{47}$$

where $V_{exch}^{(0)}$ is the volume part of the interaction, and

$$\mathscr{M}_{exch}(F, GT) = \left\langle \Psi_{A,B}^{(f)} || (1,\ \sigma)\tau || \Psi_{A,B}^{(i)} \right\rangle$$

are Fermi (F) or Gamow-Teller (GT) matrix elements for the nuclear transition. One certainly expects deviations from the PWBA, and $B(GT)$ values extracted using Eq. (45) can become inaccurate. This equation has been widely used in the literature, although it is known to fail in some situations. It can be used with caution to infer electron capture, beta-decay, or neutrino scattering response functions in nuclei from charge-exchange reactions (Bertulani and Lotti 1997).

The validity of one-step processes in Eq. (44) is a reasonable assumption for (p, n) reactions. But, in heavy-ion charge-exchange reactions, this might not be as appropriate, as shown in Refs. Lenske et al. (1989), Bertulani (1993). Multistep processes including the physical exchange of a proton and a neutron

were considered in Ref. (Lenske et al. 1989) and shown to be relevant up to 100 MeV/nucleon. Deviations from Eq. (44) are common under many circumstances (Bertulani and Lotti 1997). For GT transitions comprising a small fraction of the sum rule, a direct proportionality between σ(p, n) and $B(GT)$ values does not exist. Discrepancies have also been observed (Watson et al. 1985) in reactions with odd-A nuclei including ^{13}C, ^{15}N, ^{35}Cl, and ^{39}K and in charge exchange with heavy ions (Steiner et al. 1996).

Double Charge-Exchange and Double Beta-Decay

A more ambitious reaction probe involves *double charge-exchange reactions*, seen schematically in Fig. 8. They may be used to extract matrix elements for *double beta-decay in nuclei* for a number of energetically allowed decays. In the DWBA, amplitude for this process involves the matrix element

$$\mathscr{M}(\mathbf{k},\mathbf{k}') = \sum_{\gamma,\mathbf{k}''} C_\gamma \left\langle \chi^{(-)}_{\mathbf{k}'} \left| V_{exch} \frac{1}{E_{\mathbf{k}} - \varepsilon_{\gamma,\mathbf{k}''} - T - V_{exch}} V_{exch} \right| \chi^{+}_{\mathbf{k}} \right\rangle, \tag{48}$$

where $\chi_{\mathbf{k}}$ is the distorted scattering wave in an optical potential U, $\mathbf{k}$, $\mathbf{k}'$ are the initial and final scattering momenta, $\mathbf{k}''$ is the momentum of an intermediate state γ with energy $\varepsilon_{\gamma,\mathbf{k}''}$, and T is the kinetic energy operator. C_γ includes spectroscopic amplitudes of the intermediate states. At forward scattering angles and using the same approximations as in Eq. (47), a proportionality also emerges between double charge-exchange reactions and double beta-decay processes. The typical cross sections in a single-step charge-exchange reaction are a few millibarns, whereas a double charge-exchange cross section is expected to be less than microbarns (Bertulani 1993).

Double beta-decay is typically ground-state to ground-state transitions, accompanied by two neutrino emissions or by no neutrino emission. In the latter scenario, they place constraints on particle physics beyond the standard model, involving

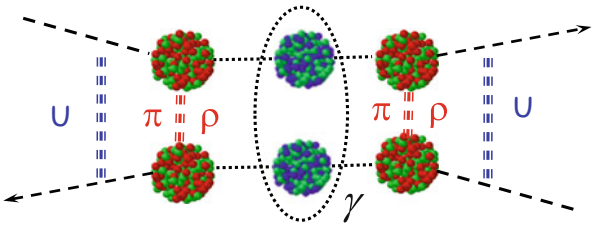

Fig. 8 Schematic description of a double charge-exchange reaction, where a two-step process is induced by the nucleon-nucleon interaction. The optical potential U is responsible for the elastic scattering of the incoming and outgoing nuclei, whereas the charge exchange is viewed as pion+rho exchange in nucleon-nucleon interactions

concepts such as lepton number nonconservation and the neutrino being a Majorana particle, e.g., its own antiparticle. Neutrinoless double beta-decay studies involve the neutrino mass and complicated nuclear transition matrix elements. Double beta-decays into two neutrinos have been observed (Elliott et al. 1987), but neutrinoless double beta-decay still remains elusive in experimental nuclear physics.

Fermi-type operators do not contribute appreciably to double beta-decay when neutrinos are emitted, because the ground state of the final nucleus is not a double isobaric analog of its initial state. Hence, the relevant transitions are of double Gamow-Teller type. In neutrinoless beta-decay, Gamow-Teller are expected to be larger than Fermi transitions (Zheng et al. 1990). Using double charge-exchange reactions as a probe of double beta-decay matrix elements is now being pursued by many experimental groups (see, e.g., Matsubara et al. 2013; Kisamori et al. 2016; Cappuzzello et al. 2018) not only for assessing neutrinoless double beta-decay but also to study exotic nuclear structures (see, e.g., Lenske et al. 2018; Shimizu et al. 2018).

Figure 9 shows that a correlation seems to exist between calculated *double charge-exchange* (DCE) nuclear matrix elements (NMEs) for Gamow-Teller (GT) transitions and neutrinoless double beta-decay ($0\nu\beta\beta$) (adapted from Ref. Santopinto et al. 2018). The calculations have been performed for ^{116}Cd $\rightarrow$ ^{116}Sn, ^{128}Te $\rightarrow$ ^{128}Xe, ^{82}Se $\rightarrow$ ^{82}Kr, and ^{76}Ge $\rightarrow$ ^{76}Se. The nearly linear correlation can be explained with a transparent reaction theory, and if it remains robust, it

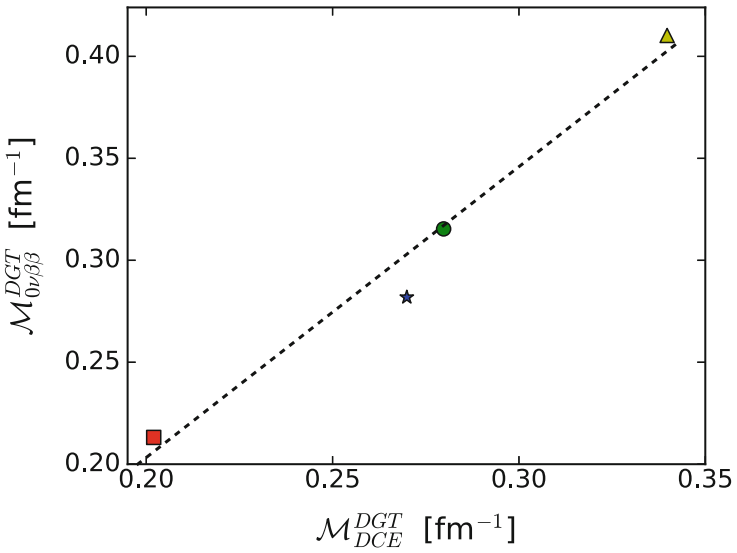

Fig. 9 Correlation between the calculated double charge-exchange (DCE) nuclear matrix elements (NMEs) for Gamow-Teller (GT) transitions and for neutrinoless double beta-decay ($0\nu\beta\beta$) (Santopinto et al. 2018). The theoretical results are for ^{116}Cd $\rightarrow$ ^{116}Sn, ^{128}Te $\rightarrow$ ^{128}Xe, ^{82}Se $\rightarrow$ ^{82}Kr, and ^{76}Ge $\rightarrow$ ^{76}Se, respectively

will open the possibility of extracting neutrinoless double beta-decay NMEs from experimental data on DCE at forward angles. A recent review provides many clarifications for charge-exchange reactions as a probe of nuclear β-decay (Lenske et al. 2019).

Transfer Reactions

In the scattering of two nuclei, *nucleon transfer reactions* occur when a nucleon or a cluster of nucleons initially in a bound state of one of the two nuclei ends up in a bound state of the other nucleus. From the point of view of quantum mechanics, this happens because when the two nuclei are close together, there is a finite overlap between the tails of the initial and final wave functions. If this overlap is large, the cross section will be large compared to other reaction cross sections. For this reason transfer reactions are very selective, in particular for heavy nuclei, and they can be a very powerful spectroscopic tool. One can get information on the *spectroscopic factors* (SF) and/or *asymptotic normalization constants* (ANC) and the angular momentum quantum numbers of the wave functions. The negative single-particle binding energies of valence nucleons are known when the nucleus mass is accurately determined experimentally. However for nuclei very close to the drip line it might happen than the mass is not so well determined due to the nucleus very short time-life.

A transfer reaction can be represented as

$$A_1(a_1 + x) + A_2 \rightarrow a_1 + (A_2 + x), \tag{49}$$

where x is the transferred nucleon or cluster.

A simple classical relationship between the binding energies (ε_{n1} and ε_{n2}) and the incident energy per nucleon $\frac{1}{2}mv^2$ indicates that the optimum matching condition (Von Oertzen 1985; Bonaccorso et al. 1987; Brink 1972, 1985) is

$$|\varepsilon_{n1} - \varepsilon_{n2}| = \frac{1}{2}mv^2. \tag{50}$$

Equation (50) shows that when $\frac{1}{2}mv^2$ is very large and/or one of the binding energies is very small, then the most favored final energy for the nucleon/cluster might be positive. In this case one would talk of *transfer to the continuum* which is usually called *breakup* and that we will discuss in the following section. Furthermore, it has been shown both experimentally (Winfield et al. 1988) and theoretically (Von Oertzen 1985; Bonaccorso et al. 1987) that the transfer probability increases from the Coulomb barrier up to a maximum at an incident energy E_{crit}, given approximately by the condition

$$E_{crit} = |Q| - V_{CB}/A_{12}, \tag{51}$$

where Q is the reaction Q-value, $V_{CB} = Z_1 Z_2 e^2/R_s$ is the value of the projectile-target Coulomb barrier at the strong absorption radius R_s, and $A_{12} = A_1 A_2/(A_1 + A_2)$.

At high energies the transfer probability decreases with the angular momentum and spin of the initial and final state. The spin dependence of the transfer probability is influenced both by the reaction Q-value and by the spin coupling factors between initial and final states. Classical arguments suggest (Buttle and Goldfarb 1971; Brink 1972) that spin-flip transitions ($j_1 = l_1 \pm \frac{1}{2} \rightarrow j_2 = l_2 \mp \frac{1}{2}$) are favored at low incident energies, while the opposite occurs at high energies. The inversion from one regime of spin selectivity to the other occurs when $E_{inc} \approx E_{crit}$. On the other hand, because the angular momentum must be conserved, the difference between the initial and final angular momenta must be provided by the relative motion angular momentum, such that (Brink 1972)

$$\hbar(\lambda_1 - \lambda_2) = \left| \frac{R Q_{eff}}{v} \right| \tag{52}$$

where Q_{eff} takes into account the Coulomb barriers and R is close to the sum of the radii of projectile and target. If the *matching conditions* are not satisfied, the cross sections for transfer are going to be depleted with respect to other competing channels.

Following the discussion of transfer reactions contained in (Aumann et al. 2021), Figs. 10 and 11 show two examples of the momentum matching condition. Figure 10 contrasts the neutron-adding (d, p) and (α,^{3}He) reactions on ^{60}Ni, while Fig. 11 compares the neutron-removing (p,d) and (^{3}He,α) reactions on ^{76}Se (Schiffer et al. 2008) and (Schiffer et al. 2013). In the first example, the beam energies were about 5 MeV/nucleon for the (d,p) reaction and 9.5 MeV/nucleon for the (α,^{3}He) reaction, both being near the peak cross sections, as seen in Fig. 10. These results are consistent with some previous works on heavy ion scattering (Winfield et al. 1988; Von Oertzen 1985; Bonaccorso et al. 1987).

From Fig. 11, bottom part, the energy spectra for the two reactions, (d,p) and (α,^{3}He), appear to be very different. The momentum matching condition, shown in the inset, indicates $RQ_{eff} \approx 1$ for the (d, p) reaction and ≈ 4 for the (α,^{3}He) reaction. The ratios of the cross sections between the two reactions for ℓ=1 or 4 differ by nearly two orders of magnitude depending on their ℓ value. This is an astonishing demonstration that momentum matching occurs. We thus understand that the cross sections from the respective reactions are low (high) because of poor (good) momentum matching. When the matching is poor, the contributions of more complicated, indirect (multistep) pathways can contribute more significantly, and the interpretation of the cross section being a simple one-step process becomes questionable. As a result the structure information extracted, such as the spectroscopic factors, for example, will not be reliable.

Transfer observables can be calculated with the DWBA theory or with semi-classical methods which are obtained from the previous when certain conditions apply. First we derive the formulae for the angular distributions in DWBA theory.

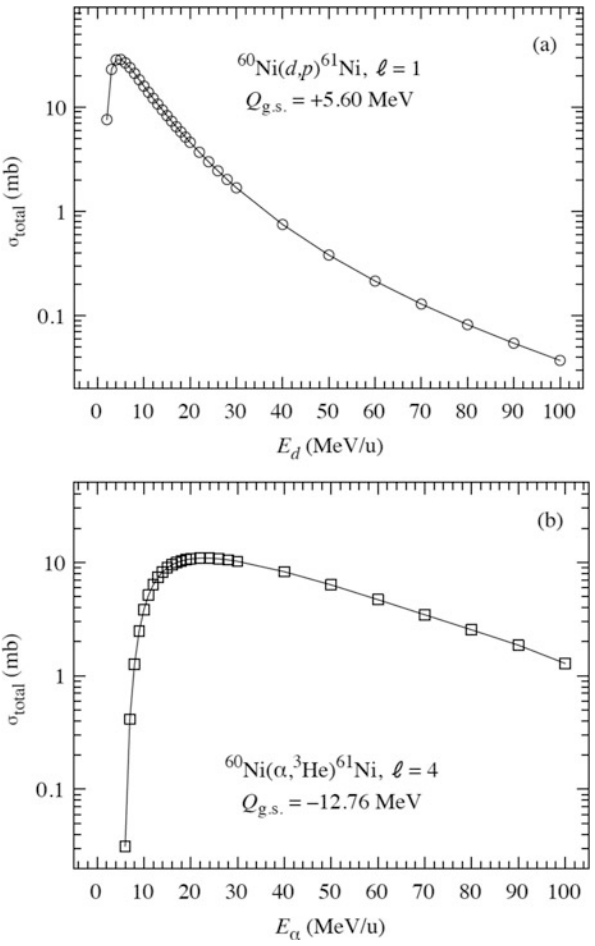

Fig. 10 Energy dependence of two reactions, ^{60}Ni(d,p) and ^{60}Ni(α,p), showing a peak at the critical energy. See text for details

The scattering amplitude for a reaction $A_1(A_2, a_1)a_2$ in the center-of-mass frame is

$$T_{\mathrm{DWBA}}(\theta, \phi) = -\frac{\mu_\beta}{2\pi\hbar^2} \int\int \chi_\beta^{(-)}(\mathbf{k}_{\boldsymbol{\beta}}, \mathbf{r}_{\boldsymbol{\beta}})^* \left\langle \mathrm{a}_1, \mathrm{a}_2 \left| V_{eff} \right| \mathrm{A}_1, \mathrm{A}_2 \right\rangle \chi_\alpha^{(+)}(\mathbf{k}_{\boldsymbol{\alpha}}, \mathbf{r}_{\boldsymbol{\alpha}}) \mathrm{d}\mathbf{r}_{\boldsymbol{\beta}}, \tag{53}$$

where the functions χ_α and χ_β are distorted waves describing the elastic scattering of the particles in the entrance ($\alpha = \mathrm{A}_1 + \mathrm{A}_2$) and exit ($\beta = \mathrm{a}_1 + \mathrm{a}_2$) channels, with momentum and relative coordinates $\mathbf{k}_{\boldsymbol{\alpha},\boldsymbol{\beta}}$ and $\mathbf{r}_{\boldsymbol{\alpha},\boldsymbol{\beta}}$, respectively. V_{eff} denotes the interaction inducing the transition, and μ_β is the reduced mass in the exit channel.

It follows that the cross section for a *single-particle (s.p.) state*, with a certain angular momentum and orbital angular momentum transfer, is

$$\frac{d\sigma(\theta)}{d\Omega} = \frac{v_\beta}{v_\alpha} \left| T_{\mathrm{DWBA}}(\theta) \right|^2, \tag{54}$$

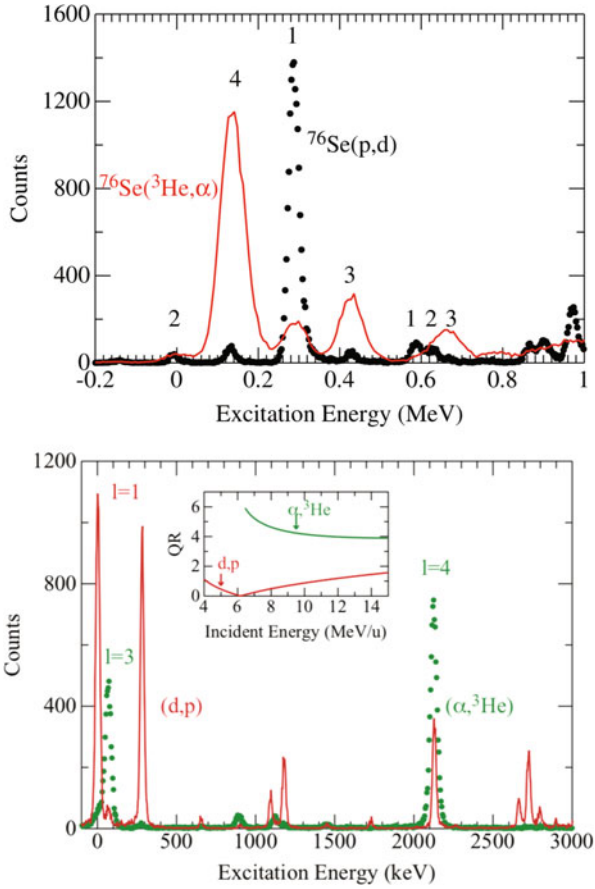

Fig. 11 Spectra from the neutron-adding (p, d) and (^{3}He,α) reactions, top figure, and neutron-removing (d, p) and (α,^{3}He) reactions, bottom figure. Shown in the inset is the momentum matching which indicates $RQ_{eff} \approx 1$ for the (d, p) reaction and $RQ_{eff} \approx 4$ for the (α,^{3}He) reaction. The ratios of the cross sections between the two reactions for $\ell = 1$ or 4 differ by about two orders of magnitude depending on their ℓ value demonstrating the effect of the momentum matching

where v_α and v_β are the center-of-mass velocities in the incoming and outgoing channels.

In Eq. (53), the matrix element $\langle a_1, a_2 \left| V_{eff} \right| A_1, A_2 \rangle$ includes an integral over the internal coordinates of the many-body wave functions of the incident and outgoing particles. It is common to assume that V_{eff} does not depend on the internal coordinates. For example, if a_2 emerges from the addition of one neutron to the target A_2, one needs to perform the *overlap integral*

$$\int d\xi \; \Psi^*_{a_2}(\xi, \mathbf{r}) \Psi_{A_2}(\xi) \equiv \psi^{\ell,j}_{A_2 a_2}(\mathbf{r}), \tag{55}$$

where ξ stands for the internal coordinates of A and $\mathbf{r}$ that of the additional neutron. This overlap integral is proportional to the probability amplitude to find the state a_1 when a nucleon is removed from A_1. Generally, $\psi^{\ell,j}_{A_1 a_1}(\mathbf{r})$ is not normalized to one. Its normalization yields the so-called spectroscopic factor:

$$\int d\mathbf{r} |\psi^{\ell,j}_{A_1 a_1}(\mathbf{r})|^2 = S^{\ell,j}_{A_1 a_1}. \tag{56}$$

In practical calculations using the DWBA, the overlap function is often approximated by a *single-particle* $(s.p.)$ *wave function*, obtained from the solution of a Schrödinger equation with a mean-field potential (such as a Woods-Saxon type), with the appropriate separation energy and quantum numbers ℓ, j. Since the $s.p.$ wave function is unit normalized, one writes

$$\psi^{\ell,j}_{A_1 a_1}(\mathbf{r}) \approx \sqrt{S^{\ell,j}_{A_1 a_1}}\, \psi^{\ell,j}_{sp}(\mathbf{r}), \tag{57}$$

where $\psi^{\ell,j}_{sp}(\mathbf{r})$ is the $s.p.$ wave function.

With explicit account of the angular momentum, additional *Clebsch-Gordan coefficients* appear in the formalism. In addition, if the isospin formalism is used to express the states A and B, another *isospin coefficient* (C) appears. They are sometimes singled out from the definition of the spectroscopic factors and hence written explicitly as (C^2S). The use of Clebsch-Gordan coefficients in the context of transfer reactions is thoroughly discussed in Ref. (Schiffer 1969), and an explicit example is given in Ref. (Szwec et al. 2016). C^2 is often taken as one and not discussed at length or maybe intentionally or unintentionally ignored.

If the $s.p.$ overlap Eq. (57) is included in the scattering amplitude, Eq. (53), one may write the differential cross section as a $s.p.$ cross section multiplied by a respective spectroscopic factor, i.e.,

$$\frac{d\sigma(\theta)}{d\Omega} = \omega\,(C^2 S_i)\, \left.\frac{d\sigma(\theta)}{d\Omega}\right|_{\rm sp}, \tag{58}$$

where S_i is the spectroscopic factor for the specific state i. Notice that, if both the projectile and target overlap functions are written in terms of $s.p.$ overlaps, a product of the corresponding spectroscopic factors will appear in Eq. (58). An additional *statistical factor* ω is needed, which is $(2j+1)$ for adding and one for removing nucleons.

The angular distributions obtained in this way are characterized by oscillations that depend on the transferred angular momentum, and thus their measure has been routinely used to determine l-values for the final (initial) $s.p.$ states. This is most easily done in (d,p) and (α,^{3}He) reactions because in this case the initial angular momentum is zero. On the other hand, heavy ion reactions are useful when one wants to study final states of high spins because they are favored in this case due to the large relative angular momentum. However, in heavy ion reactions, there are other channels competing with transfer; thus the underlying core-target interaction is quasi-elastic and coupled-channels calculations are necessary. For these reasons, at present most of the time, one prefers to use (d,p) reactions.

Breakup Reactions

In the previous section, we have argued that *breakup reactions* have the same physical origin as transfer reactions and that they become dominant when following Eq. (50) the most favored nucleon or cluster final energy is positive. According to quantum mechanics (QM), positive energies give rise to a continuum spectrum. Therefore, breakup can be seen as a transfer reaction in which all final energies are possible. In transfer reactions the nucleon final-state wave function is determined only by the final nucleus potential. On the other hand, in breakup reactions the particle final state is in the continuum; the particle will have final-state interactions with both the initial and final nucleus potentials; thus in principle its wave function should reflect both these potentials. Clearly, breakup is more complicated than transfer but at the same time can give more information on the two interacting nuclei, and it all depends on the measured observables.

In an *exclusive reaction*, the breakup particle is measured in coincidence with the core of origin, then one has access to the continuum spectrum of the original nucleus, and the energy spectrum will provide information on resonance states of the projectile. In such a case, the mechanism is the same as inelastic excitation to the continuum. In Fig. 12 we give an example for the reaction (Blanchon et al. 2007; Simon et al. 2007) ^{11}Li(^{12}C,X)^{9}Li+n at 264 MeV/nucleon. The data and theoretical analysis give information on the low-lying resonances of the unbound nucleus ^{10}Li

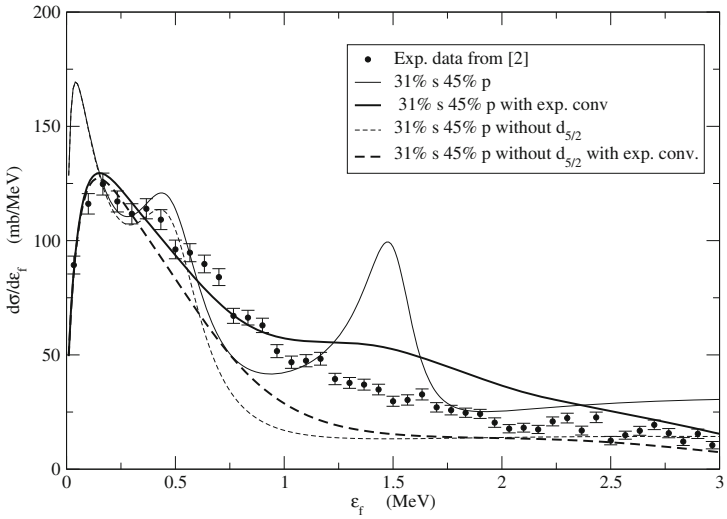

Fig. 12 Relative-energy spectrum n-^{9}Li following ^{11}Li projectile fragmentation in the reaction (Blanchon et al. 2007; Simon et al. 2007) ^{11}Li(^{12}C,X)^{9}Li+n at 264 MeV/nucleon. The inset details how the data and theoretical analysis yields information on the low-lying resonances of the unbound nucleus ^{10}Li and on the corresponding components of the two-neutron halo nucleus ^{11}Li ground-state wave function

and on the corresponding components of the two-neutron halo nucleus ^{11}Li ground-state wave function.

In an *inclusive reaction*, only the original core is measured. A continuum energy spectrum is obtained which contains mainly information on the final-state interaction of the breakup particle with the target. If the target final state is not determined, the spectrum contains the effect of both elastic and inelastic scattering similarly to what is discussed in previous sections for a beam of free particles. However, because in the initial state the particle is bound, the treatment needs special care. Some examples are given in Fig. 13. On the top part of the figure, the spectra are given as a function of the core final momentum. Their shape and width give information on the angular momentum and separation energy of the nucleon in the initial state. The figure at the bottom shows an energy spectrum for the target plus one neutron. It is obtained from the projectile-core energy (*missing mass*) measurement after the collision. One can see the presence of low-lying resonances as well as a large bump due to the re-scattering of the nucleon on the target. The peak of the breakup bump or of the simple spectra at the top of the figure corresponds to the nucleon optimal final energy according to Eq. (50).

Breakup can be seen to happen because the nuclear target potential perturbs the initial bound state. When the target is very heavy and the initial state weakly bound, there is also another mechanism known as *Coulomb breakup* (Alder and Winther 1975; Bertulani and Baur 1985). It is manly due to the recoil of the core which generates a dipole potential such that there is an effective Coulomb force acting on the breakup particle. Typical measurements consist in taking in coincidence the breakup particle and its core. However because the effect of the nuclear potential is always present, the formalism must take care of the interference between the two mechanisms (Bonaccorso 2018). For example, Coulomb breakup must be taken into account in reactions involving the weakly bound deuteron unless the other nucleus involved is very light.

Breakup reactions have been extensively studied from the early 1980s when it was noticed that in a systematic of reaction cross sections of helium, beryllium, and lithium projectiles in correspondence to some isotopes (^{6}Be,^{11}Be,^{11}Li), the cross sections showed an unexpected enhancement (Tanihata et al. 1985) (see Fig. 14). This is due to the weakly bound valence neutrons and thus to the strong effect of the breakup channel. For the same nuclei and the same reason, the effect of breakup can also be seen on the elastic scattering angular distributions, in the form of a depletion of elastic scattering cross sections with respect to neighboring nuclei, as shown by Fig. 2.

The theoretical treatment of breakup is in principle very complicated because, at least in DWBA, an expression like Eq. (53) must be solved with a three-body final state which would take into account the nucleon-core, nucleon-target, core-target nuclear potentials plus the core-target Coulomb interaction and, if the breakup particle or cluster is charged, its Coulomb interaction with core and target. However, there is possibly a simplification due to the fact that large breakup cross sections are measured only for peripheral reactions which apart from the breakup are otherwise

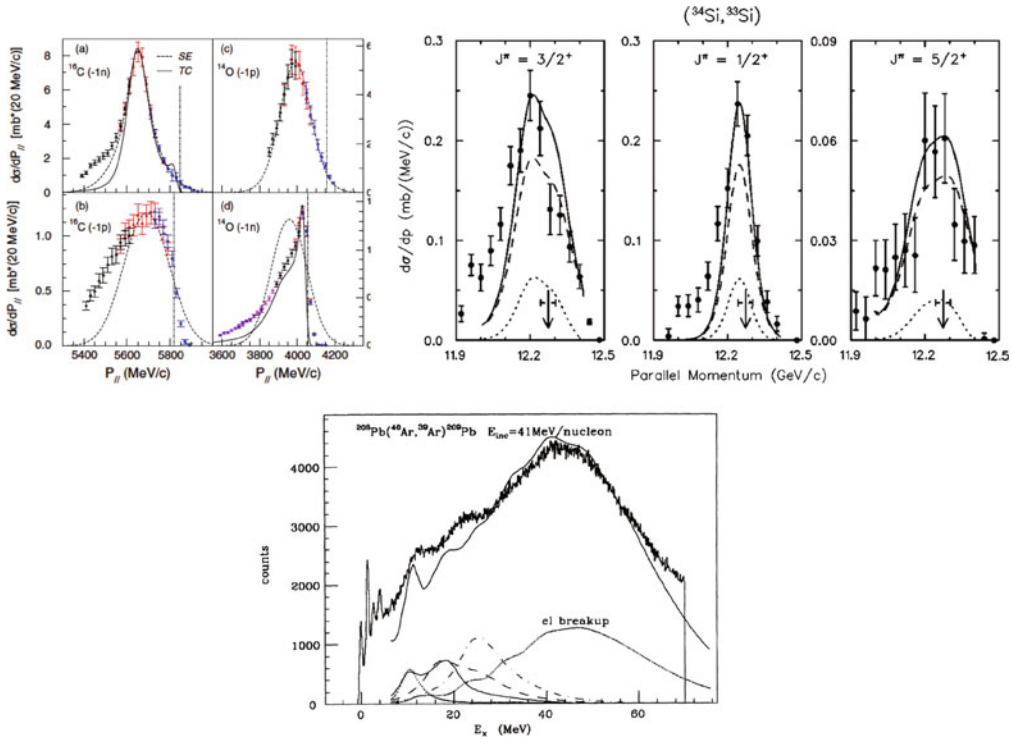

Fig. 13 Examples of momentum and energy spectra taken from Refs. Bonaccorso et al. (1994), Enders et al. (2002), Flavigny et al. (2012). The top left panel shows the parallel-momentum distributions of the core of ^{16}C and ^{14}O after nucleon removal due to interactions with a ^{9}Be target at 80 MeV/nucleon. Data are from Ref. (Flavigny et al. 2012). The curves display the results of different theoretical models. On the top panel right, the same sort of distributions are shown for the reaction ^{9}Be(^{34}Si,^{33}Si) at 69 MeV/nucleon. Data are from Ref. (Enders et al. 2002). The bottom panel shows the energy spectra of the fragments in the reaction ^{208}Pb(^{40}Ar,^{39}Ar) at 41 MeV/nucleon (Bonaccorso et al. 1994)

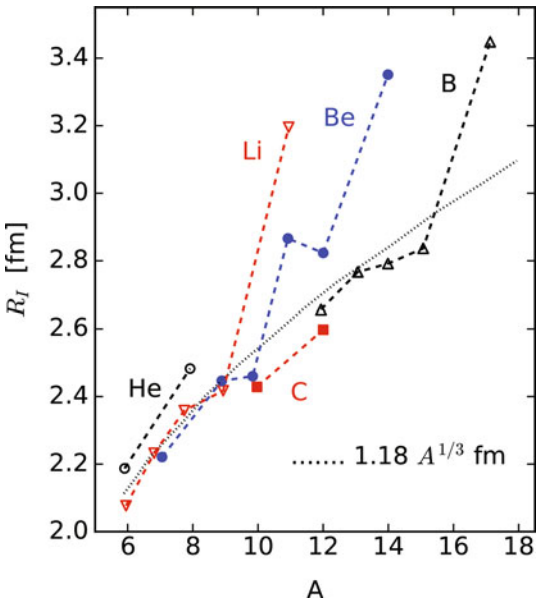

Fig. 14 Experimentally extracted interaction radii of light nuclei, determined from the interaction cross sections. The interaction radius (R_I) is defined by $\sigma_I = \pi(R_I^P + R_I^T)^2$, where P and T denote the projectile and target, respectively. A sudden increase of matter radii is seen for nuclei near neutron drip line (Tanihata 1996)

quasi-elastic. At small impact parameters instead channels other than breakup take over, and thus the exact value of the breakup cross section is not important. In such circumstances the core and nucleon behaviors can be decoupled, the so-called core-spectator model applies, and the final cross section can be represented semiclassically by an integration over core-target impact parameters

$$\frac{d\sigma_{-n}}{d\zeta} = C^2 S \int d^2\mathbf{b_c} |S_{CT}(\mathbf{b_c})|^2 \frac{dP_{-n}(\mathbf{b_c})}{d\zeta}. \tag{59}$$

In Eq. (59) the variable ζ can be the nucleon final energy in the continuum, if $\varepsilon_{n2} > 0$ in Eq. (50) and/or the nucleon relative momentum with respect to the core or target given by four-energy momentum conservation (see, e.g., Firk 2010) and the relative Jacobian. The differential cross section $d\sigma_{-n}/d\zeta$ then becomes directly comparable to the measured momentum distributions function of $P_{//}$, the core parallel momentum, as in the spectra at the top of Fig. 13. If a shell model Woods-Saxon wave function is used for the initial nucleon wave function, C^2S is the spectroscopic factor of the initial state exactly as in Eq. (58). In the core-spectator model, the breakup cross section is obtained by integrating the differential breakup probability on the core-target impact parameter b_c by weighting it with the probability $|S_{CT}(b_c)|^2$ that the measured core has survived "intact" the scattering. Breakup reactions substitute transfer as spectroscopic tools whenever in Eq. (50) the most favorite final energy is positive $\varepsilon_{n2} > 0$. This typically happens when $\varepsilon_{n1} << \frac{1}{2}mv^2$.

In the following we will give three expressions for the breakup probability $dP_{-n}(b_c)/d\zeta$ which would be used to calculate spectra as those in Figs. 12 and 13, respectively. The energy spectrum of a breakup nucleon with respect of its core of origin is given by an inelastic excitation-like expression:

$$\frac{dP_{in}}{d\varepsilon_{n2}} = \mathscr{C}\frac{1}{2l_1+1}\Sigma_{m_1,m_2}|1-\bar{S}_{m_1,m_2}|^2|I_{m_1,m_2}|^2, \tag{60}$$

where $\mathscr{C}$ contains various kinematical factors and $\bar{S}_{m_1,m_2} = \exp[2i(\delta+\nu)]$ is a nucleon-core off-the-energy-shell S-matrix which depends on the nucleon-core phase shift δ but contains also an extra phase ν due to the initial bound state. $|I|^2 \sim e^{-2\gamma b_c}/b_c^3$ can be interpreted as an inelastic-like form factor, and it is interesting to compare it to the transfer to the continuum form factor $e^{-2\eta b_c}/b_c$ given in the following expression. The inelastic form factor decreases with the impact parameter much faster than the transfer/breakup form factor. This is a well-known characteristic for final bound states (Broglia and Winther 1991), and it would be interesting to see that it persists for final continuum states in future studies.

The nucleon-target energy spectrum can be calculated with

$$\frac{dP_{-n}}{d\varepsilon_{n2}} \approx \frac{1}{2}\Sigma_{j_2}(2j_2+1)(|1-S_{j_2}|^2+1-|S_{j_2}|^2)\frac{e^{-2\eta b_c}}{2\eta b_c}\mathscr{F}_{n2,n1}, \tag{61}$$

where S_{j_2} is the free particle S-matrix obtained with a proper nucleon-target optical potential, η is a kinematical factor, and $\mathscr{F}_{n2,n1}$ contains various initial and final states kinematical and spin variables. $e^{-2\eta b_c}/2\eta b_c$ can be seen as a breakup form factor. The two terms proportional to $|1-S_{j_2}|^2$ and $(1-|S_{j_2}|^2)$ represent the elastic and inelastic re-scattering of the nucleon on the target. These are indicated by the dotted and dashed curves in the top RHS spectra of Fig. 13.

If the eikonal approximation is used, the previous equation becomes

$$\frac{dP_{-n}(\mathbf{b_c})}{dk_1} = \int d^2\mathbf{b}_{n2}(|1-S(\mathbf{b}_{n2})|^2+1-|(\mathbf{b}_{n2})|^2)|\tilde{\psi}_{n1}(|\mathbf{b}_{n2}-\mathbf{b}_c|,k_1)|^2, \tag{62}$$

where, as in the transfer case, ψ_{n1} is the initial-state single-particle wave function. In the previous expression, it enters via its one-dimensional Fourier transform with respect to $k_1 = (\varepsilon_{n2}-\varepsilon_{n1}-\frac{1}{2}mv^2)/\hbar v$ which is the nucleon parallel-momentum component with respect to the core. Energy and momentum conservation implies that the core parallel-momentum distribution in the laboratory is

$$P_{//} = \sqrt{(T_p+\varepsilon_{n1}-\varepsilon_{n2})^2+2M_r(T_p+\varepsilon_{n1}-\varepsilon_{n2})},$$

such that a measurement of the latter gives a direct information on the momentum distribution of the valence particle in the initial state of the projectile. T_p is the projectile kinetic energy and M_r the residual mass. Thus, inserting Eq. (62)

in Eq. (59), the cross section differential with respect to the intrinsic parallel momentum in the core is obtained in the full eikonal formalism. Finally, by transforming in terms of the core *parallel-momentum distribution* $P_{//}$, the cross section becomes comparable to the measured spectrum.

Conclusions

In this review, we have chosen to discuss only a small subset of properties and features of direct nuclear reactions. Many subjects were left out and only very general aspects for specific cases have been discussed. Direct nuclear reactions have been a cornerstone tool to probe nuclear structure and continuously are used in new studies involving radioactive nuclear beams. In fact, nucleon removal and breakup reactions have been used for a long time to infer basic properties of nuclei, leading to some surprises, as shown in Fig. 14, where the large nuclear matter extension in the so-called halo nuclei was first identified. This finding was the seed of a new era in nuclear physics, allowing for the development of new theoretical formulations for direct nuclear reactions involving weakly bound nuclei. Direct nuclear reactions is still a very active field in nuclear physics both as an experimental tool of choice and as a playground for new ideas and developments in nuclear reaction theory.

Acknowledgments This work has been supported in part by the US DOE grant No. DE-FG02-08ER41533.

References

K. Alder, A. Winther, *Coulomb Excitation* (Academic Press, New York, 1965)
K. Alder, A. Winther, *Electromagnetic Excitation: Theory of Coulomb Excitation with Heavy Ions* (North-Holland, Amsterdam, 1975)
A.N.F. Aleixo, C.A. Bertulani, Coulomb excitation in intermediate-energy collisions. Nucl. Phys. A **505**, 448 (1989)
T. Aumann, C.A. Bertulani, Indirect methods in nuclear astrophysics with relativistic radioactive beams. Progr. Particle Nucl. Phys. **112**, 103753 (2020)
T. Aumann, C. Barbieri, D.C. Bazin, A. Bertulani, A. Bonaccorso, W.H. Dickhoff, A. Gade, M. Gomez-Ramos, B.P. Kay, A.M. Moro, T. Nakamura, A. Obertelli, K. Ogata, S. Paschalis, T. Uesaka, Quenching of single-particle strength from direct reactions with stable and rare-isotope beams. Prog. Part. Nucl. Phys. **118**, 103847 (2021)
P. Axel, Electric dipole ground-state transition width strength function and 7-MeV photon interactions. Phys. Rev. **126**(2), 671–683 (1962)
V. Bernard, N. Van Giai, Effects of collective modes on the single-particle states and the effective mass in 208pb. Nucl. Phys. A **348**(1), 75–92 (1980)
G. Bertsch, J. Borysowicz, H. McManus, W.G. Love, Interactions for inelastic scattering derived from realistic potentials. Nucl. Phys. A **284**(3), 399–419 (1977)
C.A. Bertulani, Heavy-ion charge exchange in the Eikonal approximation. Nucl. Phys. A **554**, 493–508 (1993)
C.A. Bertulani, Relativistic continuum-continuum coupling in the dissociation of halo nuclei. Phys. Rev. Lett. **94**, 072701 (2005)

C.A. Bertulani, G. Baur, Relativistic Coulomb collisions and the virtual radiation spectrum. Nucl. Phys. A **442**, 739–752 (1985)
C.A. Bertulani, G. Baur, Electromagnetic processes in relativistic heavy ion collisions. Phys. Rep. **163**(5), 299–408 (1988)
C.A. Bertulani, P. Danielewicz, *Introduction to Nuclear Reactions* (IOP, Bristol, 2004)
C.A. Bertulani, P. Lotti, Fermi and Gamow-Teller strength in charge exchange with radioactive beams. Phys. Lett. B **402**(3), 237–242 (1997)
C.A. Bertulani, A.M. Nathan, Excitation and photon decay of giant resonances from high-energy collisions of heavy ions. Nucl. Phys. A **554**(1), 158–172 (1993)
H. Bethe, S.T. Butler, Phys. Rev. **85**, 1045 (1952)
G. Blanchon et al., ^{10}Li spectrum from ^{11}Li fragmentation. Nucl. Phys. A **791**(3), 303–312 (2007)
A. Bonaccorso, Direct reaction theories for exotic nuclei: an introduction via semi-classical methods. Progr. Particle Nucl. Phys. **101**, 1–54 (2018)
A. Bonaccorso et al., Nucleon transfer in heavy-ion reactions: energy dependence of the cross section. J. Phys. G Nucl. Phys. **13**(11), 1407–1428 (1987)
A. Bonaccorso et al., Inclusive spectra of stripping reactions induced by heavy ions. Phys. Rev. C **49**, 329–337 (1994)
D.M. Brink, *Some Aspects of the Interaction of Fields with Matter*. Ph.D. Thesis, Balliol College, University of Oxford, Unpublished, 05 1955
D.M. Brink, Kinematical effects in heavy-ion reactions. Phys. Lett. B **40**(1), 37–40 (1972)
D.M. Brink, *Semi-Classical Methods in Nucleus-Nucleus Scattering* (Cambridge University Press, Cambridge, 1985)
R.A. Broglia, A. Winther, *Heavy Ion Reactions, Lecture Notes*. Frontiers in Physics, vol. 84 (Addison-Wesley Publishing Company, New York, 1991)
P.J.A. Buttle, L.J.B. Goldfarb, Systematics of nucleon transfer between heavy ions at low energies. Nucl. Phys. A **176**(2), 299–320 (1971)
L.F. Canto, M.S. Hussein, *Scattering Theory of Molecules, Atoms and Nuclei* (World Scientific, Singapore, 2013)
F. Cappuzzello, C. Agodi, M. Cavallaro, D. Carbone, S. Tudisco, D. Lo Presti, J.R.B. Oliveira, P. Finocchiaro, M. Colonna, D. Rifuggiato, L. Calabretta, D. Calvo, L. Pandola, L. Acosta, N. Auerbach, J. Bellone, R. Bijker, D. Bonanno, D. Bongiovanni, T. Borello-Lewin, I. Boztosun, O. Brunasso, S. Burrello, S. Calabrese, A. Calanna, E.R. Chávez Lomelí, G. D'Agostino, P.N. De Faria, G. De Geronimo, F. Delaunay, N. Deshmukh, J.L. Ferreira, M. Fisichella, A. Foti, G. Gallo, H. Garcia-Tecocoatzi, V. Greco, A. Hacisalihoglu, F. Iazzi, R. Introzzi, G. Lanzalone, J.A. Lay, F. La Via, H. Lenske, R. Linares, G. Litrico, F. Longhitano, J. Lubian, N.H. Medina, D.R. Mendes, M. Moralles, A. Muoio, A. Pakou, H. Petrascu, F. Pinna, S. Reito, A.D. Russo, G. Russo, G. Santagati, E. Santopinto, R.B.B. Santos, O. Sgouros, M.A.G. da Silveira, S.O. Solakci, G. Souliotis, V. Soukeras, A. Spatafora, D. Torresi, R. Magana Vsevolodovna, A. Yildirim, V.A.B. Zagatto, The numen project: Nuclear matrix elements for neutrinoless double beta decay. Eur. Phys. J. A **54**(5), 72 (2018)
D. Cline, Nuclear shapes studied by Coulomb excitation. Ann. Rev. Nucl. Part. Sci. **36**, 683 (1986)
A. Di Pietro, G. Randisi, V. Scuderi, L. Acosta, F. Amorini, M.J.G. Borge, P. Figuera, M. Fisichella, L.M. Fraile, J. Gomez-Camacho, H. Jeppesen, M. Lattuada, I. Martel, M. Milin, A. Musumarra, M. Papa, M.G. Pellegriti, F. Perez-Bernal, R. Raabe, F. Rizzo, D. Santonocito, G. Scalia, O. Tengblad, D. Torresi, A. Maira Vidal, D. Voulot, F. Wenander, M. Zadro, Elastic scattering and reaction mechanisms of the halo nucleus ^{11}Be around the coulomb barrier. Phys. Rev. Lett. **105**, 022701 (2010)
T. Druet, P. Descouvemont, Continuum effects in the scattering of exotic nuclei. Eur. Phys. J. A **48**(10), 147 (2012)
F.F. Duan et al., Scattering of the halo nucleus ^{11}Be from a lead target at 3.5 times the Coulomb barrier energy. Phys. Lett. B **811**, 135942 (2020)
S.R. Elliott, A.A. Hahn, M.K. Moe, Direct evidence for two-neutrino double-beta decay in ^{82}Se. Phys. Rev. Lett. **59**, 2020–2023 (1987)
J. Enders et al., Single-neutron knockout from ^{34,35}Si and ^{37}S. Phys. Rev. C **65**, 034318 (2002)

H. Fesbach, *Theoretical Nuclear Physics: Nuclear Reactions* (Wiley, London, 1992)
H. Feshbach, The optical model and its justification. Ann. Rev. Nucl. Sci. **8**, 49 (1958)
F.W.K. Firk, Introduction to relativistic collisions (2010). arXiv:1011.1943
F. Flavigny et al., Nonsudden limits of heavy-ion induced knockout reactions. Phys. Rev. Lett. **108**, 252501 (2012)
M.A. Franey, W.G. Love, Nucleon-nucleon t-matrix interaction for scattering at intermediate energies. Phys. Rev. C **31**, 488–498 (1985)
R.J. Glauber, Lectures in theoretical physics, in ed. by W.E. Brittin, L.C. Dunham, vol. 1 (Interscience, New York, 1959)
J. Goldstone, Derivation of the Brueckner many-body theory. Proc. R. Soc. Lond. A **239**(1217), 267–279 (1957)
L.C. Gomes, J.D. Walecka, V.F. Weisskopf, Properties of nuclear matter. Ann. Phys. **3** 241 (1958)
M.S. Hussein, R.A. Rego, C.A. Bertulani, Microscopic theory of the total reaction cross section and application to stable and exotic nuclei. Phys. Rep. **201**(5), 279–334 (1991)
J.-P. Jeukenne, A. Lejeune, C. Mahaux, Optical-model potential in finite nuclei from Reid's hard core interaction. Phys. Rev. C **16**, 80–96 (1977)
K. Kisamori, S. Shimoura, H. Miya, S. Michimasa, S. Ota, M. Assie, H. Baba, T. Baba, D. Beaumel, M. Dozono, T. Fujii, N. Fukuda, S. Go, F. Hammache, E. Ideguchi, N. Inabe, M. Itoh, D. Kameda, S. Kawase, T. Kawabata, M. Kobayashi, Y. Kondo, T. Kubo, Y. Kubota, M. Kurata-Nishimura, C.S. Lee, Y. Maeda, H. Matsubara, K. Miki, T. Nishi, S. Noji, S. Sakaguchi, H. Sakai, Y. Sasamoto, M. Sasano, H. Sato, Y. Shimizu, A. Stolz, H. Suzuki, M. Takaki, H. Takeda, S. Takeuchi, A. Tamii, L. Tang, H. Tokieda, M. Tsumura, T. Uesaka, K. Yako, Y. Yanagisawa, R. Yokoyama, K. Yoshida, Candidate resonant tetraneutron state populated by the ^{4}He(^{8}He,^{8} Be) reaction. Phys. Rev. Lett. **116**, 052501 (2016)
H. Lenske, H.H. Wolter, H.G. Bohlen, Reaction mechanism of heavy-ion charge-exchange scattering at intermediate energies. Phys. Rev. Lett. **62**, 1457–1460 (1989)
H. Lenske, J.I. Bellone, M. Colonna, J.-A. Lay, Theory of single-charge exchange heavy-ion reactions. Phys. Rev. C **98**, 044620 (2018)
H. Lenske, F. Cappuzzello, M. Cavallaro, M. Colonna, Heavy ion charge exchange reactions as probes for nuclear β-decay. Progr. Particle Nucl. Phys. **109**, 103716 (2019)
C. Mahaux, R. Sartor, Dispersion relation approach to the mean field and spectral functions of nucleons in 40ca. Nucl. Phys. A **528**(2), 253–297 (1991)
H. Matsubara, M. Takaki, T. Uesaka, S. Shimoura, N. Aoi, M. Dozono, T. Fujii, K. Hatanaka, T. Hashimoto, T. Kawabata, S. Kawase, K. Kisamori, Y. Kikuch, Y. Kubota, C.S. Lee, H.C. Lee, Y. Maeda, S. Michimasa, K. Miki, H. Miya, S. Noji, S. Ota, S. Sakaguchi, Y. Sasamoto, T. Suzuki, L. T. Tang, K. Takahisa, H. Tokieda, A. Tamii, K. Yako, Y. Yasuda, N. Yokota, R. Yokoyama, J. Zenihiro, Spectroscopic measurement in ^{9}He and ^{12}Be. Few-Body Syst. **54**(7), 1433–1436 (2013)
S. Mordechai et al., Pion double charge exchange to the double dipole resonance. Phys. Rev. Lett. **61**, 531–534 (1988)
J.M. Mueller, R.J. Charity, R. Shane, L.G. Sobotka, S.J. Waldecker, W.H. Dickhoff, A.S. Crowell, J.H. Esterline, B. Fallin, C.R. Howell, C. Westerfeldt, M. Youngs, B.J. Crowe, R.S. Pedroni, Asymmetry dependence of nucleon correlations in spherical nuclei extracted from a dispersive-optical-model analysis. Phys. Rev. C **83**, 064605 (2011)
L. Ray, Proton-nucleus total cross sections in the intermediate energy range. Phys. Rev. C **20**, 1857–1872 (1979)
E. Santopinto, H. García-Tecocoatzi, R.I. Magaña Vsevolodovna, J. Ferretti, Heavy-ion double-charge-exchange and its relation to neutrinoless double-β decay. Phys. Rev. C **98**, 061601 (2018)
G.R. Satchler, *Direct Nuclear Reactions* (Clarendon Press, Oxford, 1983)
J.P. Schiffer, *Isospin in Nuclear Physics*, ed. by D.H. Wilkinson (North-Holland, Amsterdam, 1969)
J.P. Schiffer, S.J. Freeman, J.A. Clark, C. Deibel, C.R. Fitzpatrick, S. Gros, A. Heinz, D. Hirata, C.L. Jiang, B.P. Kay, A. Parikh, P.D. Parker, K.E. Rehm, A.C.C. Villari, V. Werner, C. Wrede,

Nuclear structure relevant to neutrinoless double β decay: ^{76}Ge and ^{76}Se. Phys. Rev. Lett. **100**, 112501 (2008)
J.P. Schiffer, C.R. Hoffman, B.P. Kay, J.A. Clark, C.M. Deibel, S.J. Freeman, M. Honma, A.M. Howard, A.J. Mitchell, T. Otsuka, P.D. Parker, D.K. Sharp, J.S. Thomas, Valence nucleon populations in the ni isotopes. Phys. Rev. C **87**, 034306 (2013)
R. Schmidt et al., Electromagnetic excitation of the double giant dipole resonance in ^{136}Xe. Phys. Rev. Lett. **70**, 1767–1770 (1993)
N. Shimizu, J. Menéndez, K. Yako, Double Gamow-Teller transitions and its relation to neutrinoless $\beta\beta$ decay. Phys. Rev. Lett. **120**, 142502 (2018)
H. Simon et al., Systematic investigation of the drip-line nuclei ^{11}Li and ^{14}Be and their unbound subsystems ^{10}Li and ^{13}Be. Nucl. Phys. A **791**(3), 267–302 (2007)
M. Steiner, S.M. Austin, D. Bazin, W. Benenson, C.A. Bertulani, J.A. Brown, M. Fauerbach, M. Hellström, E. Kashy, J.H. Kelley, R.A. Kryger, T. Kubo, N.A. Orr, R. Pfaff, B.M. Sherrill, M. Thoennessen, S.J. Yennello, B.M. Young, P.D. Zecher, D.J. Morrissey, C.F. Powell, First study of heavy-ion mirror charge exchange. Phys. Rev. Lett. **76**, 26–29 (1996)
S.V. Szwec et al., Rearrangement of valence neutrons in the neutrinoless double-β decay of ^{136}Xe. Phys. Rev. C **94**, 054314 (2016)
S. Hossain, M.N.A. Abdullah, Md. Zulfiker Rahman, A.K. Basak, F.B. Malik, Non-monotonic potentials for ^{6}Li elastic scattering at 88 MeV. Phys. Scr. **87**(1), 015201 (2013)
T.N. Taddeucci, C.A. Goulding, T.A. Carey, R.C. Byrd, C.D. Goodman, C. Gaarde, J. Larsen, D. Horen, J. Rapaport, E. Sugarbaker, The (p, n) reaction as a probe of beta decay strength. Nucl. Phys. A **469**(1), 125–172 (1987)
I. Tanihata, Neutron halo nuclei. J. Phys. G **22**, 157 (1996)
I. Tanihata et al., Measurements of interaction cross sections and radii of He isotopes. Phys. Lett. B **160**(6), 380–384 (1985)
W. Von Oertzen, Transfer of nucleons at high relative velocities. Phys. Lett. B **151**(2), 95–99 (1985)
S.J. Waldecker, C. Barbieri, W.H. Dickhoff, Microscopic self-energy calculations and dispersive optical-model potentials. Phys. Rev. C **84**, 034616 (2011)
J.W. Watson, W. Pairsuwan, B.D. Anderson, A.R. Baldwin, B.S. Flanders, R. Madey, R.J. McCarthy, B.A. Brown, B.H. Wildenthal, C.C. Foster, Relationship between Gamow-Teller transition probabilities and (p, n) cross sections at small momentum transfers. Phys. Rev. Lett. **55**, 1369–1372 (1985)
J.S. Winfield et al., Energy dependence of ^{12}C $+^{12}$ C single-neutron transfer cross sections. Phys. Lett. B **203**(4), 345–348 (1988)
D.-C. Zheng, L. Zamick, N. Auerbach, Nuclear structure studies of double Gamow-Teller and double beta decay strength. Ann. Phys. **197**(2), 343–375 (1990)